



Chalcone oxime derivatives as new inhibitors corrosion of carbon steel in 1 M HCl solution

A. Thoume^{a,b}, D. Benmessaoud Left^a, A. Elmaksoudi^b, F. Benhiba^c, A. Zarrouk^{d,*}, N. Benzbiria^a, I. Warad^e, M. Dakir^b, M. Azzi^a, M. Zertoubi^a

^aLaboratoire Interface Matériaux Environnement (LIME), Faculté des Sciences Ain Chock, Université Hassan II de Casablanca, B.P 5366, Morocco

^bLaboratoire de Synthèse Organique, Extraction et Valorisation (LSOEV), Faculté des Sciences Ain Chock, Université Hassan II de Casablanca, B.P 5366, Morocco

^cLaboratory of Advanced Materials and Process Engineering, Faculty of Sciences, Ibn Tofail University, BP 242, 14000 Kenitra, Morocco

^dLaboratory of Materials, Nanotechnology and Environment, Faculty of Sciences, Mohammed V University in Rabat, Av. Ibn Battouta, P.O. Box. 1014, Agdal-Rabat, Morocco

^eDepartment of Chemistry and Earth Sciences, P.O. Box 2713, Qatar University, Doha, Qatar

ARTICLE INFO

Article history:

Received 24 February 2021

Revised 21 April 2021

Accepted 1 May 2021

Available online 5 May 2021

Keywords:

Chalcone oxime derivatives

Carbon steel corrosion

Weight loss-electrochemical techniques

SEM/UV-visible

Theoretical calculations

ABSTRACT

In this research, 1,3-diphenylprop-2-en-1-one oxime (CO) and 4-nitrophenyl-1-phenylprop-2-en-1-one (CO-NO₂) was synthesized and its adsorption properties and corrosion inhibition ability was evaluated for carbon steel (CS) in 1 M HCl at 293–323 K temperature using chemical and electrochemical techniques such as weight loss measurements (WL), potentiodynamic polarization (PDP) and electrochemical impedance spectroscopy (EIS). Results evince that the inhibition activity (IE%) enhances with the compounds concentration and may achieve a maximum of 95 and 91% for CO and CO-NO₂, respectively at 293 K. In obedience with PDP findings, the tested compounds act as some mixed-type inhibitors. Survey of the temperature effect discloses that the inhibitory molecule is chemisorbed on carbon steel substrate. The adsorption of CO and CO-NO₂ occurs in accordance to the Langmuir's isotherm. Scanning Electron Microscopy (SEM) and UV-visible revealed the development of barrier film hindering the access of aggressive ions into steel surface. The theoretical findings suggested by electronic/atomic computer simulations supported the inhibitive chemicals interfacial adsorption through reactive centers.

© 2021 Elsevier B.V. All rights reserved.

1. Introduction

Corrosion is a phenomenon of considerable economic importance. It is well known that corrosion reduces the life cycle of metals [1,2], in particular steel, which is the most commonly used metal. The repair costs and high productivity losses caused by corrosion [3,4] effectively penalizes all of the industries in which acid solutions are used. The major areas of employ are pickling or acid cleaning, stimulation of oil wells, removal of localized deposits [5–8]. Owing to the aggressiveness of such acid solutions, the area of corrosion has evolved tremendously in recent years and is gradually directed towards the production of non-toxic, non-polluting and stable Corrosion inhibitors, as far as prohibition is concerned [9–11]. Corrosion inhibitors are chemicals, either inorganic or organic, that, when applied to a corrosive medium, slow the corrosion process of the exposed surface. Corrosion inhibitors are classified into two important groups: organic and inorganic compounds. Since most inorganic corrosion inhibitors are prohibited due to

their possible toxicity and contamination risk, and existing law prohibits the use of toxic substances [12–14]. Compounds organic inhibitor are the primary means of preventing metal corrosion in hostile conditions. They are typically molecules that have heteroatoms of a single pair of electrons (N, O, and S) and/or aromatic cycles of the conjugated structures π . It also has some notable features, such as multi-functionality, enhanced film shaping capabilities, and a wider surface cover [15–19]. Corrosion inhibition by organic compounds results from their adsorption on the metal by forming a protective layer on the metal surface. The adsorption phenomena can be described mainly by two interaction types, namely physical adsorption and chemisorption. Both types of adsorption are influenced by the nature and charge of the metal, the chemical structure of the organic product and the type of electrolyte [20–23]. As the current available organic corrosion inhibitors are becoming more and more dangerous, it is a matter of urgency to find new environmentally friendly inhibitors. Chalcone oxime has corrosion inhibiting properties and is therefore non-toxic, soluble in water and comparatively inexpensive [24–28].

In the present survey, the adsorption behavior and the inhibitory activity of a novel environmentally benign compound, chal-

* Corresponding author.

E-mail address: azarrouk@gmail.com (A. Zarrouk).

cone oxime derivatives, was examined for carbon steel in acidic medium (1 M HCl) at a temperature domain ranging from 293 to 323 K. In depth analysis on the adsorption mechanism of corrosion inhibitors were screened via., weight loss measurements, electrochemical techniques (PDP and EIS), as well as surface analysis by Scanning Electron Microscopy (SEM) and UV-visible were combined to evaluate the inhibition process. To gain basic findings about interactions and surface adsorption of CO and CO-NO₂, computer simulations (quantum chemistry linked with classical modeling) were applied.

2. Materials and methods

2.1. Synthesis of chalcone oxime derivatives

A mixture of chalcone derivatives (1 mmol), hydroxylamine hydrochloride (1.5 mmol), anhydrous sodium sulphate (1 mmol) was refluxed in ethanol (5 mL) while stirring (Scheme 1). Once the reaction was completed (3 h), the resulting mixture was filtrated and the solvent was subjected to evaporation at reducing pressure. Afterwards, distilled water (10 mL) and ethyl acetate (10 mL × 3) were added for the extraction of the organic products. Before filtration, anhydrous sodium sulfate was used to dry the combined organic layers. The crude product was recovered by evaporating the solvent at a low pressure. Column chromatography over silica, eluted with petroleum ether was operated to purify the product [29].

The spectral data results of chalcone oxime derivatives are gathered in Table 1.

2.2. Materials

Weight percentage composition of the tested carbon steel C38 was as follows: Fe: Base; C: 0.350–0.390; Si: ≤ 0.400; Mn: 0.50–0.80; S: 0.015–0.035; Cr + Ni + Mo: ≤ 0.63. Prior to immersion in solutions, the steel samples were polished by SiC abrasive paper having an incrementally finer grain size ranging from 200 to

1200. The specimens were then rinsed with distilled water and degreased by acetone. Samples were maintained immersed in 1 M HCl medium containing diverse inhibitor concentrations from 4.48×10^{-4} M to 2.24×10^{-3} M at a variable temperature of 293–323 K.

2.3. Weight loss measurements

Measurements of weight loss were performed in compliance with the standard methods. The specimens ($L_x = 1$ cm, $L_y = 1$ cm and $L_z = 0.3$ cm) were abraded using various abrasive papers (200–1200) and then thoroughly rinsed out with distilled water and cleansed with acetone. The carbon steel specimens were immersed in 1 M HCl solution in absence and presence of the investigated inhibitors ($4 \times 48 \cdot 10^{-4}$ to $2 \times 24 \cdot 10^{-3}$ M) at 293 K for 6 h. Afterwards, the samples were extracted and cleaned with distilled water, acetone and hot ethanol to remove all organic matter. Then, the samples were weighed and the corrosion rate (v) was determined as follows [30]:

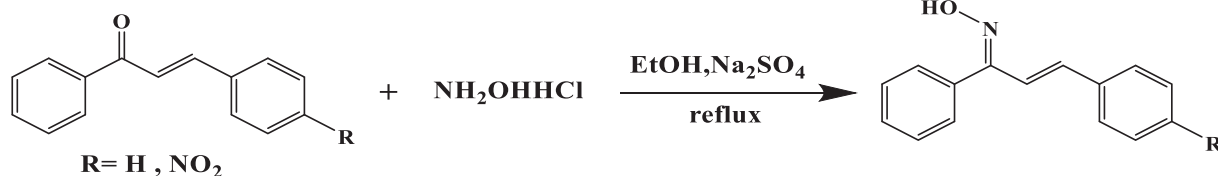
$$v = \frac{\Delta W}{S \times t} \quad (1)$$

$$\eta_w(\%) = \frac{v^0 - v}{v^0} \times 100 \quad (2)$$

where ΔW denotes the average weight loss, S represents the sample surface area (cm^2), t stands for the immersion time (h), v^0 and v designate the values of corrosion rate ($\text{mg cm}^{-2} \text{h}^{-1}$) in uninhibited and inhibited media, respectively.

2.4. Atomic adsorption measurements

This technique was operated to calculate the concentration of Fe in 1 M HCl solution without and with inhibitors (4.48×10^{-4} to 2.24×10^{-3} M) at 293 K after the electrochemical measurements. The values of the inhibition activity were determined from the atomic adsorption results according to the following formula:



Scheme 1. Synthesis of the inhibitors chalcone oxime derivatives.

Table 1
Characterization of chalcone oxime derivatives.

Molecule	Characterization
 1,3-diphenylprop-2-en-1-one oxime (CO)	¹H NMR (300 MHz, CDCl₃): δ ppm : 11.29 (s, 1H, OH), 7.78 – 7.56 (m, 4H), 7.46 – 7.31 (m, 6H), 7.29 – 6.38 (m, 2H). ¹³C NMR (75 MHz, CDCl₃): δ ppm : 157.74 (C = N); 139.76 (CH-Car), 137.04(CAr); 136.19(Cq-CH = CH), 134.79(Cq-C = N); 129.25–125.74 (CAr); 117.15(CH = CH-Cq). IR (KBr) cm⁻¹: 3450 (OH), 2300 (CH), 1620 (C = N), 1514 (C = C), 945 (N-O).
 4-nitrophenyl-1-phenylprop-2-en-1-one (CO-NO ₂)	¹H NMR (300 MHz, CDCl₃): δ ppm : 10.98 (s, 1H), 8.23 – 8.14 (m, 2H), 7.85 – 7.75 (m, 2H), 7.61 – 7.49 (m, 2H), 7.52 – 7.40 (m, 3H), 7.27 (m, 1H), 7.16 (m, 1H). ¹³C NMR (75 MHz, CDCl₃): δ ppm : 153.90 (C = N); 147.70 (C-NO ₂); 139.78(Cq-CH = CH); 135.74 (CH-CAr), 128.83(CAr); 128.59; 128.23(CAr); 127.24 (CAr) 124.60 (CAr); 123.10(CAr). IR (KBr) cm⁻¹: 3430 (OH), 2290 (CH), 1610 (C = N), 1570 (Ar-NO ₂) 1508 (C = C), 940 (N-O).

$$\eta_a(\%) = \frac{C^0 - C}{C^0} \times 100 \quad (3)$$

Here C^0 and C refer to the concentration of iron in the absence and presence respectively of CO and CO-NO₂ inhibitors.

2.5. Electrochemical measurements

The inhibitory activity of the investigated compound on carbon steel corroding were examined through Potentiodynamic Polarization (PDP) and Electrochemical impedance spectroscopy (EIS) in 1 M HCl in absence and presence of CO and CO-NO₂ concentrations going from 4.48×10^{-4} to 2.24×10^{-3} M at various temperatures 293–323 K. A classical cell with a three electrodes configuration was used in the present study. The working electrode consisted of carbon steel, whereas a platinum grid and a saturated calomel electrode (SCE) were employed as a counter and reference electrodes, respectively. Before electrochemical tests, the working electrode was immersed in 1 M HCl solution without and with different inhibitors concentrations for 40 min at open circuit potential (OCP). The PDP plots were drawn with a scan rate of 0.5 mV s^{-1} at the standard potential range found by adding $\pm 200 \text{ mV}$ to the OCP. EIS spectra were recorded between 100 kHz and 10 mHz at OCP with an amplitude of 10 mV. Three replicas of the trials were performed and the average values were regarded. The inhibitory efficacy was assessed as follows [31,32]:

$$\eta_p(\%) = \frac{i_{corr}^0 - i_{corr}}{i_{corr}^0} \times 100 \quad (4)$$

i_{corr}^0 and i_{corr} denote the corrosion current densities values in absence and presence of the inhibitory molecule, respectively.

$$\eta_{EIS}(\%) = \frac{R_p^i - R_p^b}{R_p^i} \times 100 \quad (5)$$

where R_p^b and R_p^i are polarization resistances obtained in the blank and the inhibited solutions, respectively.

The surface coverage, θ is expressed as:

$$\theta = \frac{\eta_p(\%)}{100} \quad (6)$$

η_p is the inhibitory efficiency determined by PDP.

2.6. Scanning electron microscopic measurement (SEM)

Carbon steel surface was examined after 6 h of immersion in 1 M HCl free of an inhibitor, and with the optimum concentration of CO and CO-NO₂. Carbon steel samples were transferred from the test media, rinsed with water and dried. The morphological aspect of carbon steel surface was examined by SEM (FEI FEG 450).

2.7. Computational details

2.7.1. DFT calculations

Quantum chemical calculations on the DFT approach have been carried for CO and CO-NO₂ neutral and protonated forms to provide an understanding of the key influence of molecular structures and electronic characteristics on the inhibitory properties [33]. Moreover, this complementary theoretical part has been carried out with the attempt to correlate the experimentally computed corrosion inhibition for the inhibitors with the chemical reactivity descriptors of the DFT calculations [34]. The lowest energy inhibitor shapes were tested in the DFT calculations conducted under pressure and in the gaseous phase. Additionally, the molecular structures of the compounds studied have been optimized to the

final geometry by means of the Gaussian 09 software suite at the DFT level in a functional B3LYP implementing a 6-31G (d, p) basis set [35].

The quantum descriptors like LUMO and HOMO energies, gap energy (ΔE_{gap}) (Eq. (7)), electronegativity " χ " (Eq. (8)), and other quantum descriptors such as, " η " is the global hardness which can be calculated using the Eq. (9), fraction of electrons transferred from the inhibitor molecule to the metal surface " ΔN_{110} " can be determined using Eq. (10), where the Φ work function presents the theoretical value of χ in the plan (1 1 0) of iron ($\Phi = \chi(\text{Fe}_{110}) = 4.82 \text{ eV}$) and the η represent the metallic bulk ($\eta(\text{Fe}_{110}) = 0 \text{ eV}$) [36], " ω " is the electrophilic indexes (Eq. (11)), and " ε " is the nucleophilic indexes (Eq. (12)).

$$\Delta E_{gap} = E_{LUMO} - E_{HOMO} \quad (7)$$

$$\chi = \frac{1}{2}(E_{HOMO} + E_{LUMO}) \quad (8)$$

$$\eta = \frac{1}{2}(E_{HOMO} - E_{LUMO}) \quad (9)$$

$$\Delta N_{110} = \frac{\chi_{\text{Fe}_{110}} - \chi_{\text{inh}}}{2(\eta_{\text{Fe}_{110}} + \eta_{\text{inh}})} = \frac{\Phi - \chi_{\text{inh}}}{2\eta_{\text{inh}}} \quad (10)$$

$$\omega = \frac{\chi^2}{2\eta} \quad (11)$$

$$\varepsilon = \frac{1}{\omega} \quad (12)$$

2.7.2. Molecular dynamics (MD) simulations

The adsorbed inhibitors CO and CO-NO₂ neutral and unnatural forms on the metal surface was established using the MD simulation using Forcite module implemented in Materials Studio 8.0 software [37,38]. The study of these interactions of the molecules with the Fe (1 1 0) surfaces was carried out from a simulation box ($22.34 \times 22.341 \times 35.13 \text{ \AA}^3$) with periodic boundary conditions. The Fe (1 1 0) surface was presented with a six-layer slab model in each layer representing a (11×11) unit cell. The constructed simulation box is emptied by 20.13 \AA^3 . This vacuum is occupied by $500\text{H}_2\text{O}$, $5\text{H}_3\text{O}^+$, 5Cl^- and the inhibitory molecule. The temperature of the simulated system of 293 K was controlled by the Andersen thermostat, NVT ensemble, with a simulation time of 400 ps and a time step of 1.0 fs, all under the COMPASS force field [39].

3. Results and discussion

3.1. Weight loss measurements and atomic adsorption

Table 2 displays the values of weight loss trials, the calculated corrosion rates (v), and the inhibition efficacy ($\eta_w(\%)$) values with and without diverse concentrations of CO and CO-NO₂ in 1 M HCl at a temperature of 293 K for 6 h. The analysis of Table 2 encloses the subsidence of corrosion rate and increment of the inhibitory efficiency with increasing CO and CO-NO₂ concentrations. Maximal η_w values of 95 and 92% were reached in the presence of 2.24×10^{-3} M of CO and CO-NO₂ respectively. Through the increment of the blocked portion of the steel by the synthesized inhibitors, the interaction between the metallic substrate and the destructive solution can be prevented [40]. Interestingly, identical results were found by atomic adsorption technique, where we observed that the concentration of iron decreases in 1 M HCl by the addition of CO and CO-NO₂, which main role are not only to

Table 2

Weight loss parameters and concentration of iron (ppm) in 1 M HCl containing various concentrations of CO and CO-NO₂ at 293 K.

Concentration mol/L		Weight loss			atomic adsorption	
		ΔW (mg)	v (mg cm ⁻² h ⁻¹)	η _w (%)	C (ppm)	η _a (%)
CO	Blank	11.4	1.902	—	4.776	—
	4.48 × 10 ⁻⁴	3.3	0.551	71	1.563	67
	8.96 × 10 ⁻⁴	2.5	0.418	78	1.162	76
	1.34 × 10 ⁻³	1.9	0.323	83	0.908	81
	1.79 × 10 ⁻³	1.2	0.209	89	0.686	87
	2.24 × 10 ⁻³	0.4	0.06	95	0.321	93
CO-NO ₂	4.48 × 10 ⁻⁴	3.7	0.616	68	1.688	65
	8.96 × 10 ⁻⁴	2.9	0.483	75	1.132	76
	1.34 × 10 ⁻³	1.7	0.283	85	0.733	85
	1.79 × 10 ⁻³	1.3	0.216	89	0.503	90
	2.24 × 10 ⁻³	0.9	0.150	92	0.412	91

increase the surface coverage area, but also to suppress the corrosion rate.

3.2. Electrochemical measurements

3.2.1. Potentiodynamic polarization curves

The polarization curves of the metal-solution interface are a fundamental characteristic of electrochemical kinetics but only account for the slowest stage of the overall process (transport of material, adsorption of species on the electrode. . .) at the electrochemical interface. The cathodic and anodic polarization plots of carbon steel in 1 M HCl medium without and with various concentrations of CO and CO-NO₂ are depicted in Fig. 1. Note that the curves were obtained after 40 min of immersion at E_{corr} and a temperature of 293 K. In the cathodic branch, one may notice that the curves form quasi-parallel lines, suggesting that the addition of CO and CO-NO₂ to the acidic medium does not change the mechanism of hydrogen evolution. The reduction of H⁺ ions on the carbon steel occurs primarily through electron transfer process (pure activation mechanism)[41]. From the study of Table 3 and the polarization curves reported in Fig. 1, it can be seen that the introduction of CO and CO-NO₂ induces a subsidence in both anodic and cathodic current densities, which is likely related to the prohibition of the anodic dissolution of the metal and the cathodic evolution of H₂. Besides, E_{corr} values move slightly towards more negative values and the corrosion current densities (i_{corr}) decrease as CO and CO-NO₂ concentration increases in the solution. Furthermore, both the anodic and cathodic partial currents are also decreased. These

observations confirm the mixed character of the inhibitors (lower than 85 mV) [42,43].

3.2.2. Electrochemical impedance spectroscopy measurements

Transient electrochemical methods and, in particular, electrochemical impedance spectroscopy enables to distinguish the elementary phenomena that are expected to evolve on the metal/solution interface according to their kinetics. Fig. 2 encloses the Nyquist diagrams recorded for the steel/solution interface at corrosion potential in 1 M HCl in the absence and presence of CO and CO-NO₂. Table 4 gathers the corresponding electrochemical impedance parameters. For all concentrations, the diagrams evince the presence of a single semi-circle properly centered on the axis of the impedance real part. The ray of these loops increases with increasing inhibitors concentration. In general, the feature of these type of spectra may be ascribed to charge transfer process on a heterogeneous surface [44]. An equivalent circuit (Fig. 2) is used to study the progressions involved in electrical response of the system. The capacitance double layer (Cdl), a polarization resistance (Rp) and electrical resistance (Re) forms the parts of the circuit. Through the following Eq. (13), the impedance of a constant phase element is explained. The Cdl value can be determined using Eq. (14).

$$Z_{CPE} = Q^{-1}(i\omega)^{-n} \tag{13}$$

$$C_{dl} = (Q \times R_p^{1-n})^{1/n} \tag{14}$$

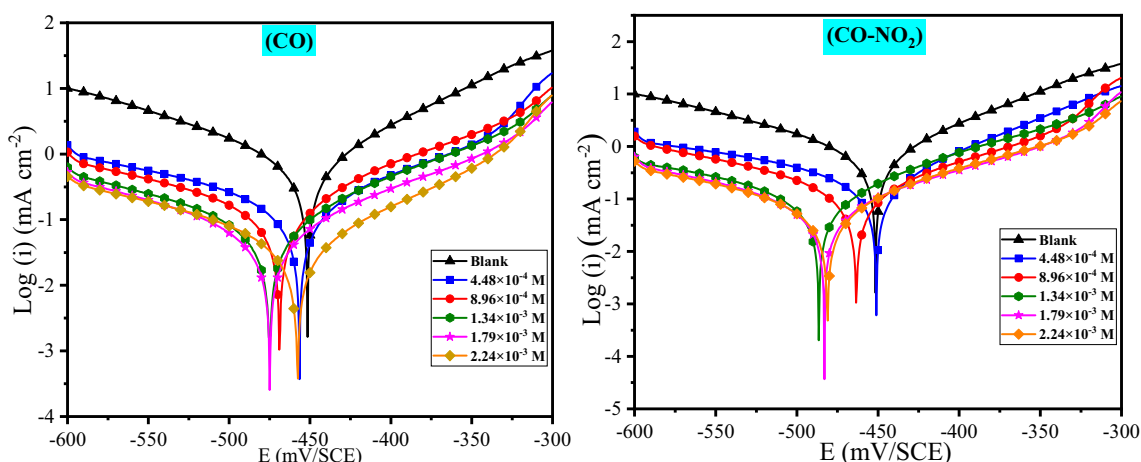


Fig. 1. Potentiodynamic polarization plots of carbon steel in 1 M HCl solution in the absence and presence of the synthesized inhibitors for 40 min at 293 K.

Table 3
Electrochemical descriptors estimated from PDP plots of carbon steel in 1 M HCl solution in the absence and presence of various concentrations of CO and CO-NO₂ at 293 K.

Concentration (mol/L)	E_{corr} (mV _{SCE})	i_{corr} (μA/cm ²)	β_a (mV dec ⁻¹)	β_c (mV dec ⁻¹)	η_p (%)	
CO	Blank	-449.7	699.9	84.4	-120.6	—
	4.48×10^{-4}	-454.6	157.9	116	-169.1	77
	8.96×10^{-4}	-466.9	146.2	105.5	-178.3	79
	1.34×10^{-3}	-473.2	081.5	100.9	-156.4	88
	1.79×10^{-3}	-473.0	0.0622	109.7	-150.1	91
	2.24×10^{-3}	-455.9	034.9	88.9	-116.8	95
CO-NO ₂	4.48×10^{-4}	-449.1	193.0	81.2	-153.8	72
	8.96×10^{-4}	-461.6	132.0	108.2	-133.5	81
	1.34×10^{-3}	-484.6	103.6	99.9	-157.0	85
	1.79×10^{-3}	-481.2	068.4	116.7	-140.1	90
	2.24×10^{-3}	-479.2	060.3	100.8	-137.6	91

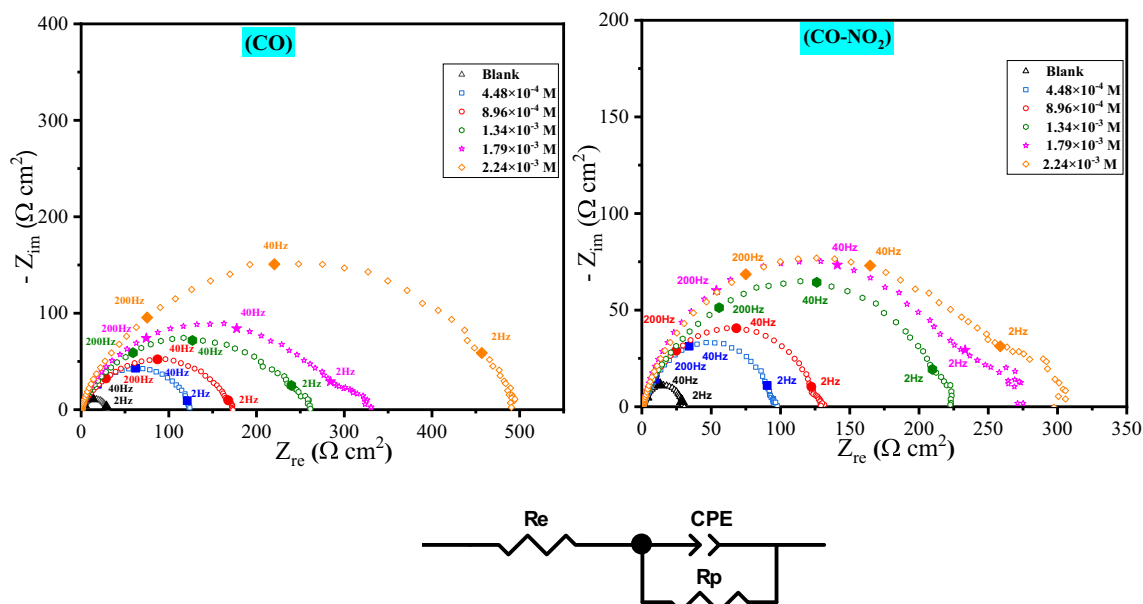


Fig. 2. Nyquist diagrams of carbon steel in 1 M HCl solution free of the inhibitor and at variance concentrations of CO and CO-NO₂ for 40 min at 293 K and the employed circuit for fitting EIS spectra.

Table 4
Electrochemical impedance descriptors of carbon steel in 1 M HCl solution comprising varied concentrations of CO and CO-NO₂ at 293 K.

Concentration (mol/L)	R_e (Ω cm ²)	R_p (Ω cm ²)	Q (μF s ⁿ⁻¹ cm ⁻²)	n	C_{dl} (μF/cm ²)	η_{EIS} (%)	χ^2	
CO	Blank	0.91	28.0	345.6	0.817	122.3	—	0.001
	4.48×10^{-4}	0.87	126.3	166.6	0.822	72.2	78	0.004
	8.96×10^{-4}	0.75	173.1	127.5	0.831	58.7	84	0.003
	1.34×10^{-3}	0.67	263.3	95.9	0.846	49.1	89	0.001
	1.79×10^{-3}	0.72	327.2	78.3	0.849	40.8	91	0.009
	2.24×10^{-3}	0.83	503.2	48.8	0.850	25.4	94	0.005
CO-NO ₂	4.48×10^{-4}	1.04	96.3	198.8	0.825	85.9	70	0.007
	8.96×10^{-4}	0.70	130.3	153.2	0.834	70.3	78	0.001
	1.34×10^{-3}	0.62	227.4	102.4	0.842	50.6	87	0.003
	1.79×10^{-3}	0.93	273.3	78.5	0.852	40.3	90	0.004
	2.24×10^{-3}	0.81	305.0	63.9	0.853	32.4	91	0.008

Where Q , i , w , and n stand for CPE constant, imaginary number, angular frequency, and phase shift, respectively. n symbolizes the deviation from the ideal behavior ranging from 0 and 1.

Chi-square element was surveyed to verify the accuracy of the fitted data. All the outcomes provided a less (10^{-3}) values of Chi-square (Table 4), mirroring the good agreement between the fitting information and the experimental finding. Polarization resistance (R_p) values and inhibitory effectiveness exhibit a significant increase as CO and CO-NO₂ concentration increases. The

trend of the inhibition ability increases in the following order: CO-NO₂(91%) < CO (94%), the lowest inhibition efficiency of the CO-NO₂ could be as a result of electron attractor nature of the -NO₂ group[45]. Another observation of Table 4 exhibits that the CPE constant Q value experienced a significant decline, which means that the CO and CO-NO₂ interact with the carbon steel electrode by occupying the vacate active sites. Further, elevation the n values of CO and CO-NO₂ relative to the uninhibited electrolyte can be related to a reduction of electrode surface roughness [46]. This

behavior is owed to the development of a protecting layer on steel substrate. Besides, the double layer capacitance subsides evidencing the adsorption of the organic compound on the metallic surface, as expressed by the Helmholtz model [47]. The lessening of C_{dl} is attributed to CO and CO-NO₂ adsorption on the steel surface, which reduces the dielectric constant of the medium ϵ , and/or increases the thickness of the electrical double layer.

$$C_{dl} = \frac{\epsilon_0 \times \epsilon}{e} \times S \text{ (Helmholtz model)} \quad (15)$$

where e represents the thickness of the deposit, S denotes the electrode surface, ϵ_0 stands for the permittivity of vacuum and ϵ designates the dielectric constant.

3.2.3. Temperature effect

The behavior of a substance in a corrosive media can be remarkably affected by temperature. In fact, metal-inhibitor interactions in a specific context can be changed. In order to assess the impact of temperature on CO and CO-NO₂ prohibition capacity, PDP curves were plotted at varied temperatures going from 293 K to 323 K. The findings are evidenced in Fig. 3 and Table 5. From Table 5, one can notice that the increment in temperature induces the enhancement of i_{corr} while the inhibitory activity stays almost stable as a consequence of the strong adsorption of the inhibitor on the metal surface (chemisorption) [48].

The influence of temperature may be explained by the Arrhenius expression between the corrosion current density and the temperature as [49,50]:

$$i_{corr} = A \times \exp\left(\frac{-E_a}{R \times T}\right) \quad (16)$$

E_a stands for the activation energy, A is defined as a pre-exponential factor, R denotes the universal gas constant and T represents the absolute temperature. The variation of the logarithm of i_{corr} as a function of the inverse of the absolute temperature yielded a straight line (Fig. 4), from which the activation energies can be computed. Table 6 evinces that the activation energy decreases in the presence of CO and CO-NO₂ compared to the blank test solution. In obedience to the classification proposed by Radovici [51], the inhibitor CO and CO-NO₂ belongs to class 2 (E_{ai} less than E_a) and acts by chemisorption.

The alternative Arrhenius relationship allow us to estimate the enthalpy and entropy energies [52]:

$$i_{corr} = \frac{R \times T}{N \times h} \times \exp\left(\frac{-\Delta S_a}{R}\right) \exp\left(\frac{-\Delta H_a}{R \times T}\right) \quad (17)$$

where h : Plank's constant, N : Avogadro's number, ΔH_a : Activation Enthalpy and ΔS_a : Activation entropy. The evolution of $\ln(i_{corr}/T)$ versus $(1/T)$ exhibits a straight line (Fig. 5). The slope and intercept correspond to $(\Delta H_a/RT)$ and $(\ln(RT/Nh + \Delta S_a/R))$, respectively. The values of enthalpies and entropies are given in the Table 6. The positive enthalpy ΔH_a signs divulges the endothermic nature of the steel dissolution process, which indicates that the anodic dissolution reaction of carbon steel is very sluggish [53]. The high and negative entropy ΔS_a value in the presence of CO and CO-NO₂ reveals

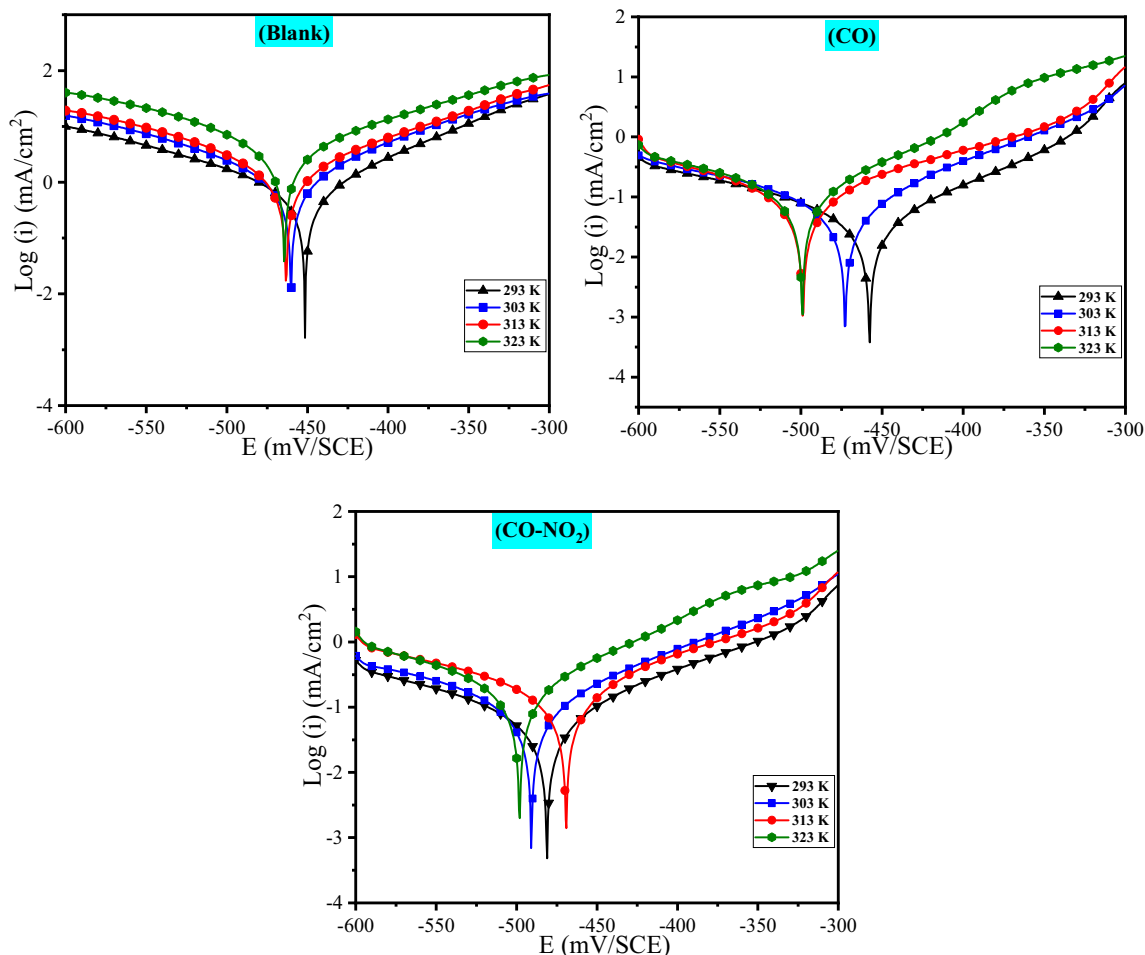


Fig. 3. PDP plots of carbon steel in 1 M HCl solution obtained in absence and the presence of 2.24×10^{-3} M of CO and CO-NO₂ at various temperatures.

Table 5
Electrochemical descriptors determined from PDP curves of carbon steel in 1 M HCl solution without and with 2.24×10^{-3} M of CO and CO-NO₂ at various temperatures.

Medium	Temperature (K)	E_{corr} (mV _{SCE})	i_{corr} (μA/cm ²)	β_a (mV dec ⁻¹)	β_c (mV dec ⁻¹)	η_p (%)
Blank	293	-449.7	699.9	84.4	-120.6	—
	303	-458.4	1206.8	95.3	-113.8	—
	313	-462.8	2272.9	185.4	-118.3	—
	323	-462.0	3717.3	117.2	-108.8	—
CO	293	-455.9	034.9	88.9	-116.8	95
	303	-470.9	075.7	101.5	-166.3	94
	313	-497.0	102.1	126.8	-143.3	96
	323	-497.2	126.3	92.5	-163.0	97
CO-NO ₂	293	-479.2	060.3	100.8	-137.6	91
	303	-489.0	104.9	104.6	-154.8	91
	313	-467.3	192.7	129.9	-198.1	92
	323	-496.3	208.5	101.5	-154.7	94

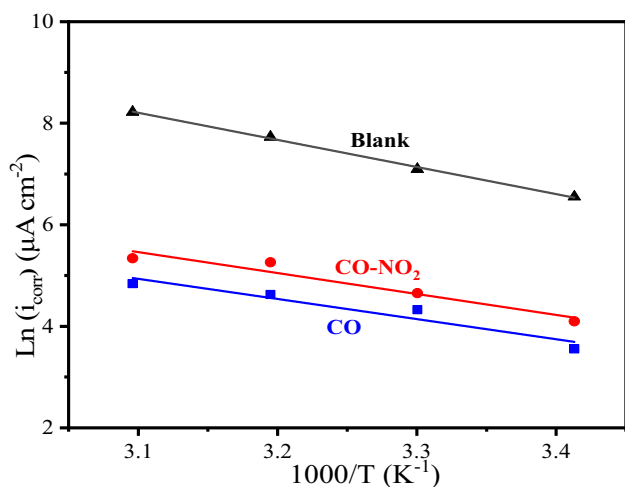


Fig. 4. Arrhenius plots for carbon steel obtained in 1 M HCl free of the inhibitor and in presence of 2.24×10^{-3} M of CO and CO-NO₂.

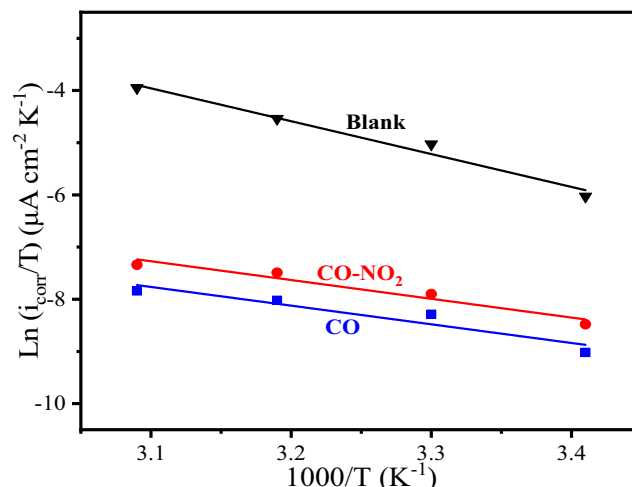


Fig. 5. $\ln(i_{corr}/T)$ versus $1000/T$ for carbon steel in 1 M HCl solution without and with 2.24×10^{-3} M of CO and CO-NO₂.

Table 6
Thermodynamic activation descriptors for carbon steel in 1 M HCl without and with 2.24×10^{-3} M of CO and CO-NO₂.

Medium	E_a (kJ mol ⁻¹)	ΔH_a (kJ mol ⁻¹)	ΔS_a (J mol ⁻¹ K ⁻¹)
Blank	43.79	41.29	-106.77
CO	32.44	29.92	-169.15
CO-NO ₂	33.83	31.29	-160.51

that the disorder is reduced when the reagents are converted to the activated iron-molecule complex in the solution [54].

3.3. Adsorption isotherm

The inhibition process of corrosion via organic substances is associated to their adsorption on the metal surface. Adsorption isotherm is an important tool to determine the electrochemical process that enables the adsorption of these organic compounds on the metallic substrate. The degree of surface coverage (θ) for varied CO and CO-NO₂ concentrations was inspected to fit various isotherms Frumkin, Langmuir and Temkin, and the correlation coefficients were operated to define the best fit. This last one was obtained with Langmuir adsorption isotherm (Fig. 6) given as [55]:

$$\frac{C}{\theta} = \frac{1}{K_{ads}} + C \tag{18}$$

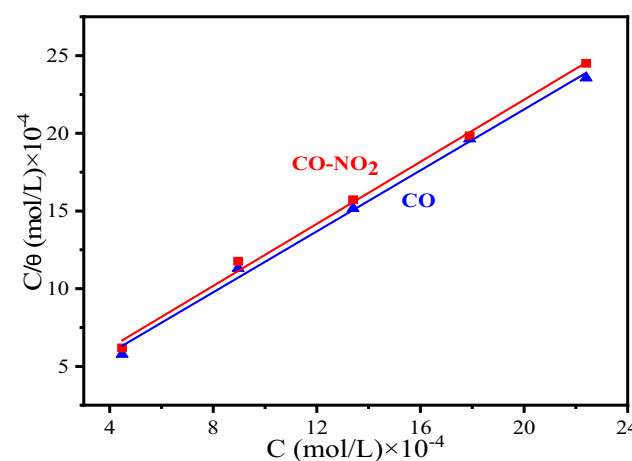


Fig. 6. Langmuir adsorption isotherm of CO and CO-NO₂ on carbon steel surface in 1 M HCl solution at 293 K.

where C designates the inhibitory molecule concentration, K_{ads} denotes the equilibrium adsorption constant and θ stands for the degree of surface coverage.

On the other hand, the free enthalpy of adsorption ΔG_{ads}° can be determined using the equation [56]:

$$K_{ads} = \frac{1}{55.5} \times \exp\left(\frac{-\Delta G_{ads}^{\circ}}{R \times T}\right) \quad (19)$$

The value 55.5 is the concentration of water. Note that ΔG_{ads}° values close to or above -20 kJ/mol are generally related to electrostatic interactions betwixt charged inhibitory molecules and metal charges (physisorption). In the other hand, values of ΔG_{ads}° near or below -40 kJ/mol correspond to a charge transfer betwixt the inhibitory molecules and the metallic substrate (chemisorption) with creation of covalent or coordination bonds. In our case, the negative value of the free adsorption energies of CO (-29.3 kJ/mol) and CO-NO₂ (-30.7 kJ/mol) discloses that the adsorption occurs spontaneously on carbon steel surface and that CO and CO-NO₂ adsorbs to the metal surface both physically and chemically (mixed adsorp-

tion)[57], with predominance of the second one since the inhibitory efficacy remains constant through temperature increase. Moreover, the high values of the equilibrium adsorption constant (3.05×10^3 M⁻¹ and 5.45×10^3 M⁻¹ for CO and CO-NO₂ respectively) indicate a strong adsorption on steel surface, which may be associated with the existence of donor atoms, such as oxygen and nitrogen[58].

3.4. Surface analysis

SEM observations were performed on carbon steel samples after 6 h immersion at 293 K in 1 M HCl without (Fig. 7a), with the addition of 2.24×10^{-3} M of CO (Fig. 7b) and with the addition of 2.24×10^{-3} M of CO-NO₂ (Fig. 7c). The SEM micrograph obtained in 1 M HCl free of the inhibitor (Fig. 7a) indicates that the surface is heavily altered as evinced by the occurrence of grey lumps and

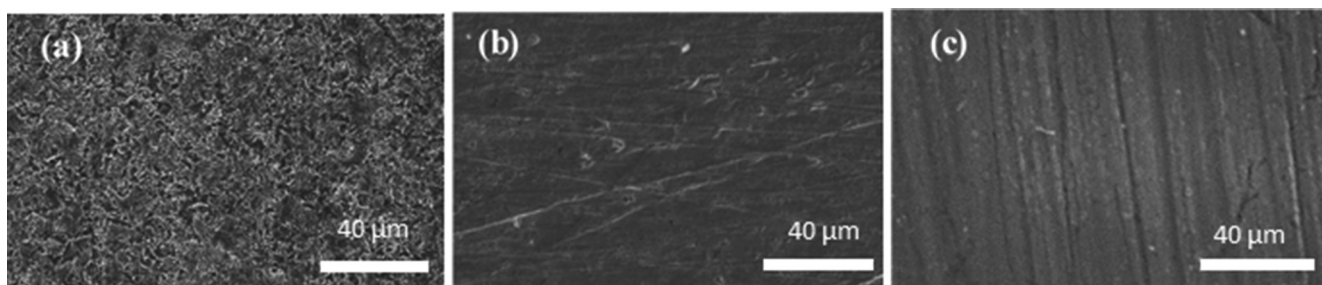


Fig. 7. SEM micrographs of carbon steel specimens after 6 h immersion in (a) 1 M HCl, (b) 1 M HCl + 2.24×10^{-3} M of CO and (c) 1 M HCl + 2.24×10^{-3} M of CO-NO₂.

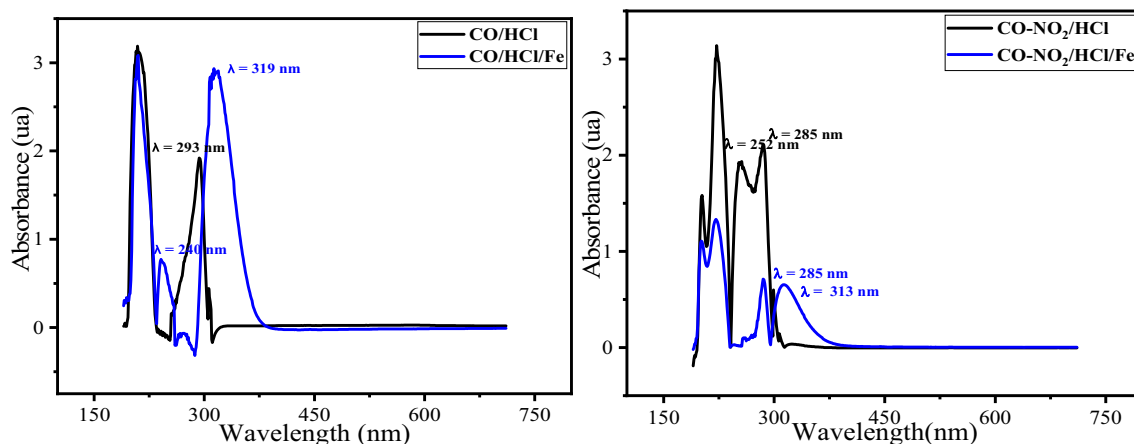


Fig. 8. UV-visible spectra of compounds CO and CO-NO₂ in HCl with and without carbon steel.

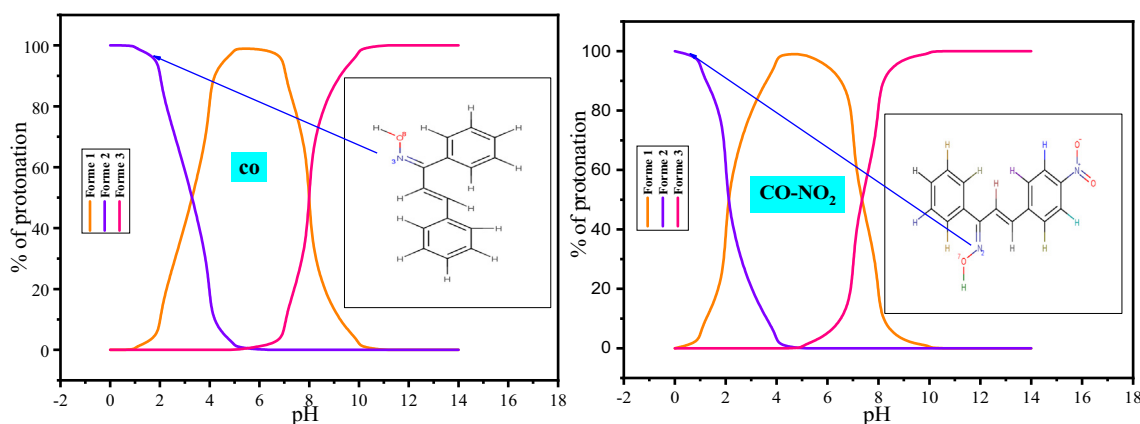


Fig. 9. Percentage of protonation of two compounds CO and CO-NO₂ vs. pH.

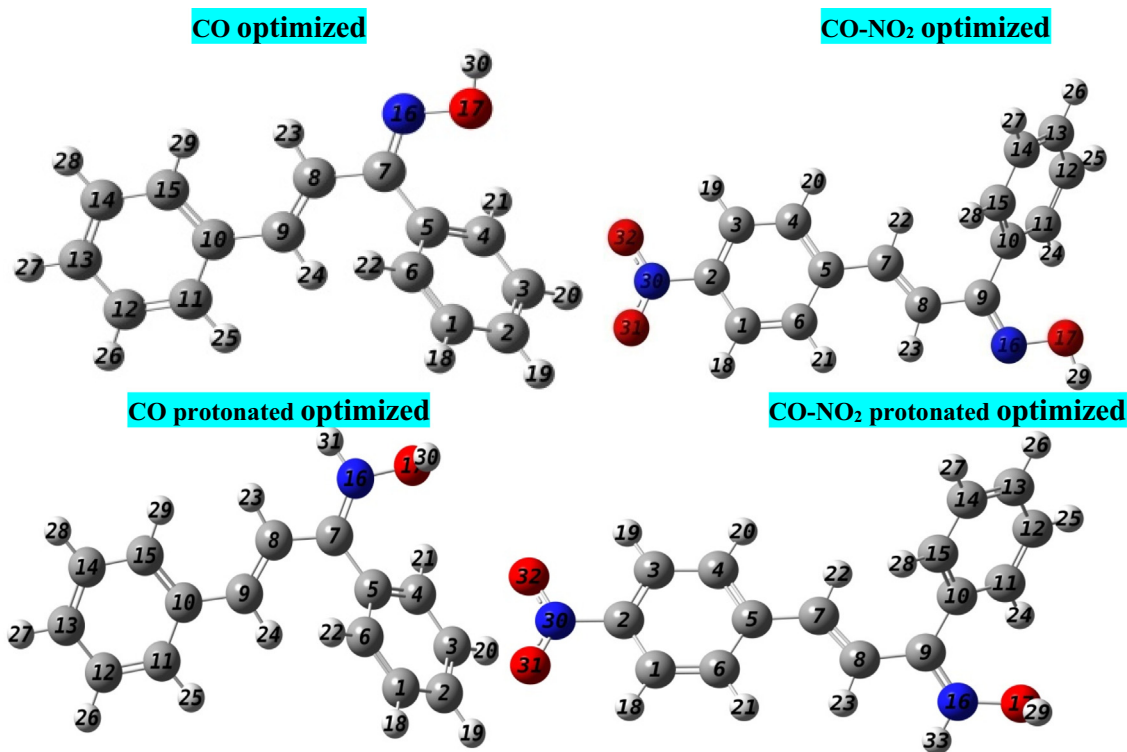


Fig. 10. Optimized geometrical skeletons of the CO and CO-NO₂ compounds in neutral and non-neutral forms.

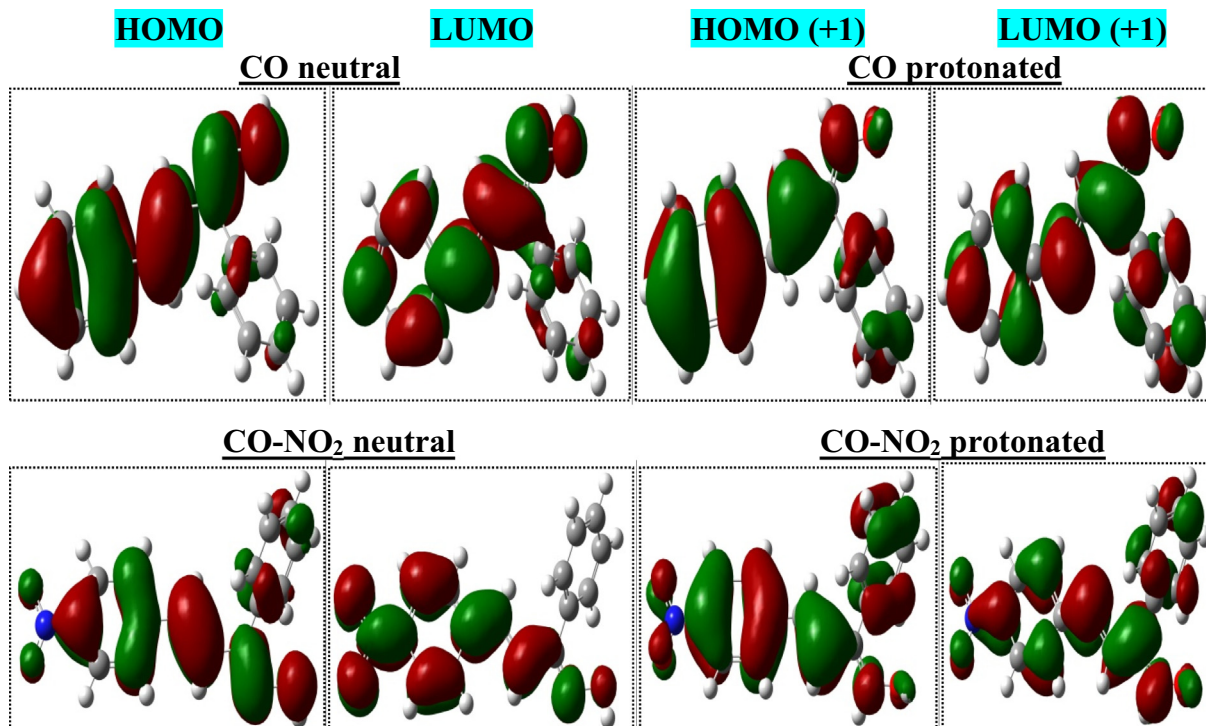


Fig. 11. HOMO-LUMO distribution densities of species CO and CO-NO₂ neutral and charged forms.

a few pitting marks (halide ions) [59]. This clearly shows that the steel undergoes practically widespread corrosion over the whole metallic surface in 1 M HCl. The grey areas likely correspond to

iron oxide films. Fig. 7b and Fig. 7c displays a smooth homogeneous surface with the addition of 2.24×10^{-3} M of CO and CO-NO₂. In comparison with the images captured without inhibitor,

Table 7
DFT-descriptors describing the reactivity of CO and CO-NO₂ no-charged and loaded forms.

Descriptors	Neutral forms		Protonated forms	
	CO	CO-NO ₂	CO	CO-NO ₂
E _{HOMO}	-5.621	-6.187	-9.951	-10.495
E _{LUMO}	-2.292	-2.615	-6.408	-6.879
ΔE _g	3.329	3.572	3.543	3.616
χ	3.956	4.401	8.179	8.687
η	1.664	1.786	1.771	1.808
ω	4.702	5.422	18.883	20.869
ε	0.213	0.184	0.053	0.048
ΔN ₁₁₀	0.259	0.117	-0.948	-1.069

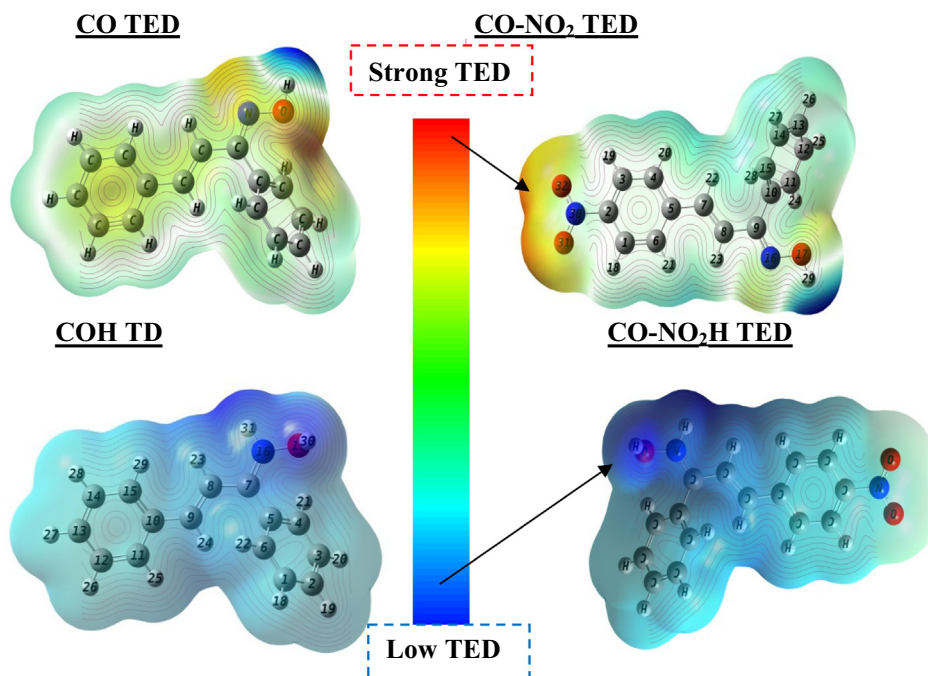


Fig. 12. TED distribution on the molecular skeleton of molecules CO and CO-NO₂ no-charged and loaded forms.

one may assume that steel surface is almost free of corrosion products in the presence of the inhibitory molecule. This is due to the development of an adsorbed film on steel surface. These observations show that the inhibitor under survey prevents the corrosion of carbon steel by limiting electrolyte access to the surface.

3.5. UV-visible characterization

To understand the nature of the bonds formed between the organic molecules, and iron ions is often obtained by UV-visible spectroscopic investigation. The change in position of the absorbance maximum and change in the value of absorbance indicate the formation of a complex between two species in solution [60]. In order to confirm the possibility of the formation of CO-Fe and CO-NO₂-Fe complex the UV-visible absorption spectra corresponding to 1 M HCl solution containing 2.24×10^{-3} M of CO and CO-NO₂, before and after 48 h of immersion of carbon steel are shown in Fig. 8 the wavelength values shift from 293 nm to 319 nm and an additional peak emerges at 240 nm for CO and also for CO-NO₂ a shift of wavelength from 252 nm to 285 nm and 285 nm to 313 nm which indicate the formation of a complex between the Fe²⁺ ions and CO, Fe²⁺ and CO-NO₂ in hydrochloric acid solution [61,62].

3.6. Electronic system behavior

The compounds studied are safe in an acidic environment and can succeed in being protonated in the heteroatoms, *i.e.* nitrogen or oxygen. In order to be more practical and efficient in the selectivity of one or both sites that are more favorable to protonation, we used the Marvin sketch software [63]. The data are reported in Fig. 9. This figure views that the nitrogen atom -C=N- (N16) is the most active site for fixing the proton H⁺. This atom can be chemically reactive, particularly in terms of its electronic behaviour within the molecular structure. The optimized geometrical skeletons of the CO and CO-NO₂ compounds in neutral and non-neutral forms are displayed in Fig. 10. These shown patterns have no negative frequencies, which suggest a particular spatial stability.

Fig. 11 gives the E-density distribution of the HOMO & LUMO of the investigated compounds. Further analysis of the distributed densities allows us to see that for neutral and charged CO and CO-NO₂ compounds, the HOMO and LUMO density is more localized over the entire structure of studied compounds except for the phenyl group (ϕ) which is attached to the C=N motif. Based on this distribution, we can predict a more accurate aid on the adsorption behavior of these species on the iron surface in the given acidic environment. In most cases, occupied and unoccupied

zones can also contain nucleophilic and/or electrophilic sites that are directly accountable for the inhibitory efficacy of CO and CO-NO₂ [64,65].

The chemical quantum descriptors calculated at the electronic level for the no-charged and loaded forms of Co and CO-NO₂ are listed in Table 7. Based on the results of this table, it is obvious that the occupied electron level HOMO (-5.621 eV) and the unoccupied level LUMO (-2.292 eV) prove the high capability of CO to donate/accept electrons in relation to Fe substrate, i.e. a great propensity to adsorb powerfully on this surface [66,67]. With regard to the influence of protonation on the electron donor–acceptor reactivity, it can be seen that the acceptor effect is more dominant than the donor effect. This can also be confirmed by the minimum values ΔE_g of CO for the two examined forms with high chemical reactivity ($\Delta E_g(\text{CO}) < \Delta E_g(\text{CO-NO}_2)$). These data can be explained by the orientation of the electrons towards the Nitro group under the attraction effect of the electrons by mesomeric action. Moreover, the great inhibition potential of CO due to its strong donor–acceptor interactions with Fe atoms can be justified by the low values of the descriptors χ and η [68]. The latter has a negative influence on the inhibitory power of compound CO-NO₂. The degree of donor electrons is judged by the number of electrons transferred ΔN_{110} which measures the ability to adsorb the selected molecules on the iron substrate [69]. The data in Table 7 shows that the higher value of ΔN_{110} (0.259) for the uncharged CO shows that this compound has a high electron donor potential to the empty orbits of the iron surface. The negative values of ΔN_{110} for the two com-

pounds found in the protonated state support the remarkable electronegativity values of these species. In addition, the electron donor effect of protonated forms no longer appears in this case. The electrophilic (ω) and nucleophilic (ϵ) indicators are also discussed and summarised in Table 7. As evidenced by the fact that the increase in the electrophilic property is higher in the case of protonated forms, involving the latter are more electron acceptors than unprotonated forms. Vice-versa, the nucleophilic form is more important in the case of neutral forms, informing more about the release of electrons [70].

Molecular electrostatic potential (MEP) is a method of showing the total electron density (TED). This method can be used to reveal the zones or regions that are liable for nucleophilic and electrophilic attacks by exploiting the different colors. In this context, the color blue signifies the sites of electrophilic attacks, while the color red shows the nucleophilic attack centers [71]. The sites of local reactivity appeared in Fig. 12. As noted, the structural surface shows several sites of electrophilic and nucleophilic attacks for both neutral forms, while the protonated form shows only electrophilic attack sites. This shows that protonation reduces electron donor sites in a remarkable manner.

An inhibitory molecule can overcome this reactivity by the existence of active sites. The nature of these bonds can be responsible for the inhibitory efficacy of the molecules treated in the acid environment [72]. In this recent study, the local selectivity of species CO and CO-NO₂ no-charged and loaded forms are calculated using Fukui functions (f_i^- ; electrophilic attack) and

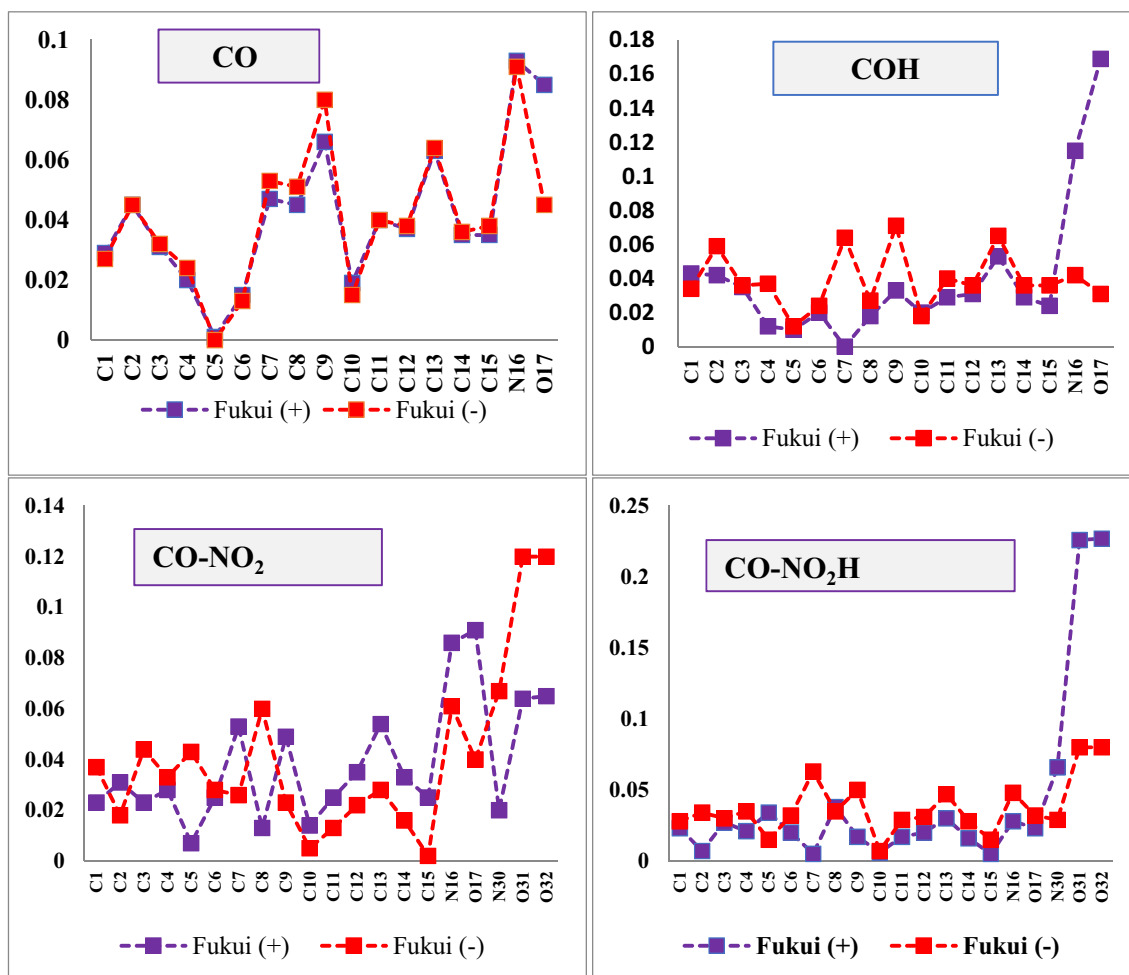


Fig. 13. f_i^- and f_i^+ for the most relevant (active) atoms of species CO and CO-NO₂ no-charged and loaded forms.

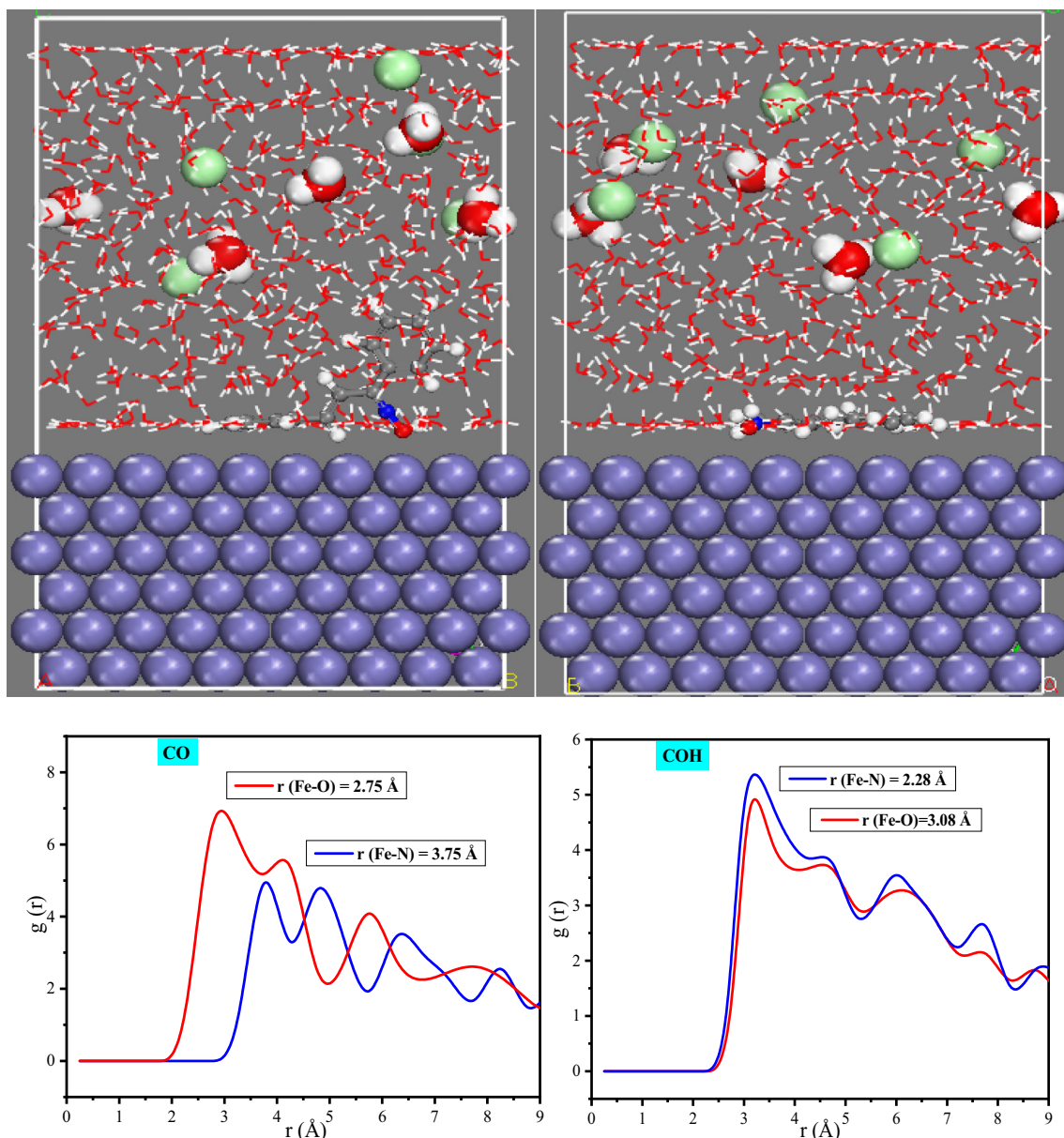


Fig. 14. MD snapshots and RDF of the preferred adsorption configuration of adsorbents in both CO and COH on the first well-ordered layer of iron.

(f_i^+ ; nucleophilic attack) with the most condensed functions present the most active centers (atoms) [73].

For this target, the generalized gradient approximation (GGA) of the Perdew-Burke-Ernzerhof (PBE) formula was taken for the correlation between the electron exchange potential and the electrons, and the all-electron calculations were conducted on a double numerical basis (DNP 4.4). f_i^- and f_i^+ are detected using the Dmol³ module in Materials Studio (ver. 8.0).

Fig. 13 allows to extract the sites of local activity, i.e. the most relevant (active) atoms of species Co and CO-NO₂ no-charged and loaded forms that are able to accept and/or give their electrons. As revealed by Fig. 13, both neutral and protonated molecules carry atoms of the same index that are either electron donor (f_i^-) or electron acceptor (f_i^+). This shows that these compounds behave in the same way with respect to adsorption reactivity on the metal surface. As recorded in the Fig. 13 the common nitrogen atom between Co and CO-NO₂ is more electron donor towards the d-

orbitals of iron. After the protonation of this site, it is quite obvious that this atom loses its electron donor power.

In general, we note that protonation influences negatively the electron donor power, while there is an increase in the acceptor power of the protonated forms. This property implies the protection of the selected steel against corrosion, indicating that the tested compounds are regarded as good corrosion inhibitors.

3.7. MD simulation

Following our study which allows us to understand the mode of action of the inhibitors tested on the steel surface in the acidic HCl medium [74,75]. Figs. 14 and 15 gives the preferred adsorption configuration of adsorbents in both neutral and protonated forms and their radial distribution functions (RDF) on the first well-ordered layer of iron. The configurations presented inform us about the adoption performance of each species on the simulated iron

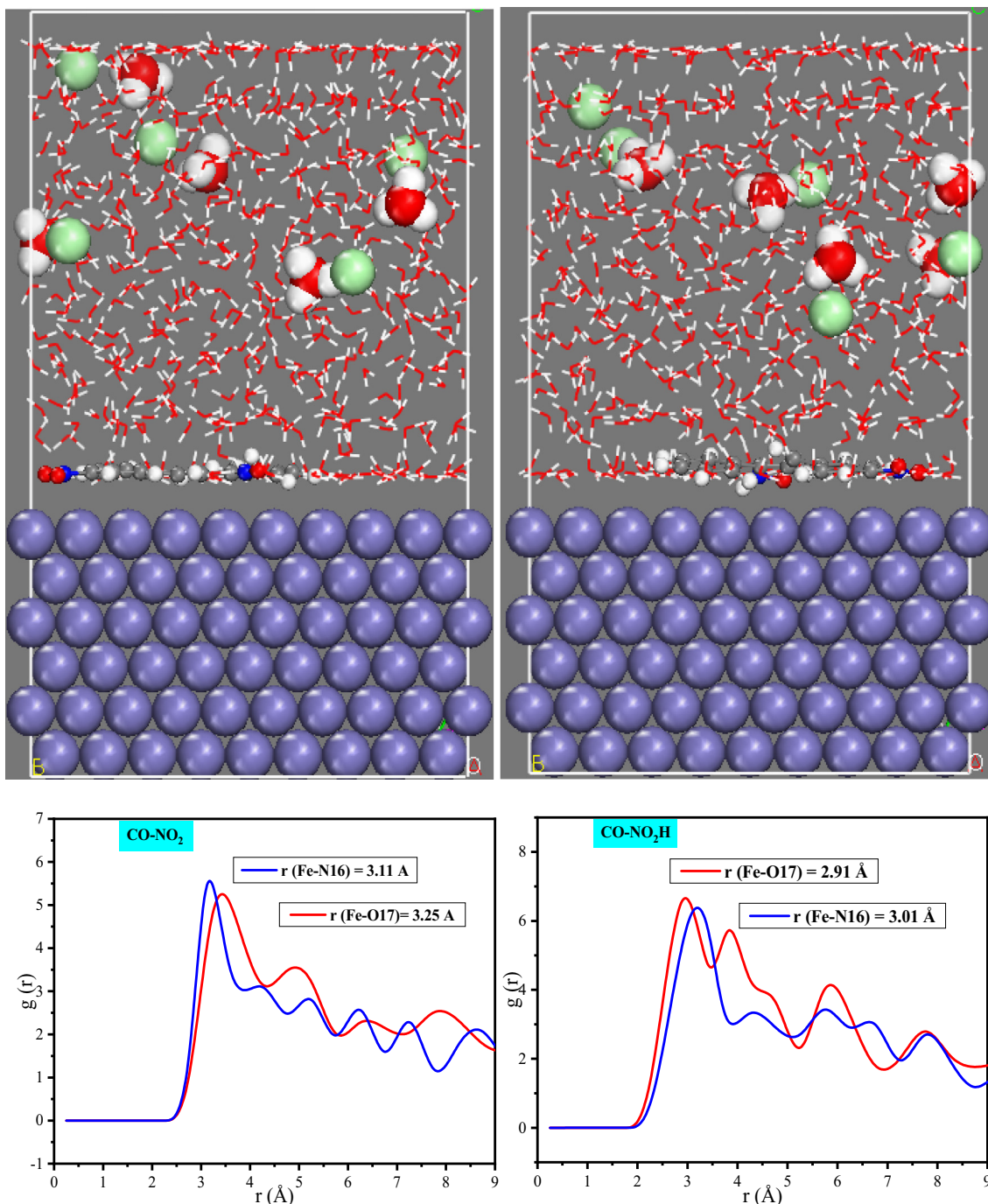


Fig. 15. MD snapshots and RDF of the preferred adsorption configuration of adsorbents in both CO-NO₂ and CO-NO₂H on the first well-ordered layer of iron.

substrate. As visualized by each configuration (Figs. 14 and 15) that the compounds COH, CO-NO₂ and CO-NO₂H adsorb through all their skeletons onto the substrate, showing that these species favor the reduction of steel metal degradation of iron in HCl. Regarding the adsorption reactivity of CO compound, it is well observed that there is a very important non-adsorbed part on the surface of the first iron layer. This behavior can negatively affect the inhibitory power of this compound.

The adsorption density field of the molecules studied in the neutral and protonated forms on the first well-ordered layer of iron is represented in Fig. 16, it is clear that a dense and hydrophobic barrier was formed to protect steel from corrosion [76].

With respect to the overviews obtained from the RDF, we can see that the values of the first peaks are lower than 3.5 Å except the bond length of Fe-N16 [77]. This shows that the species COH, CO-NO₂ and CO-NO₂H adsorb on the surface of the iron by chemical bonds, while CO adsorbs through chemical and physical bonds with the atoms of the iron in the first contact layer of the iron. These properties make it possible to reinforce the adsorption of the investigated inhibitor molecules on the surface of the metal; consequently, there is a reduction in the active sites on this area.

The interfacial interactions of species CO and CO-NO₂ non-charged and loaded forms with the Fe-surface were assessed using the interaction energy ($E_{\text{interaction}}$) [78]:

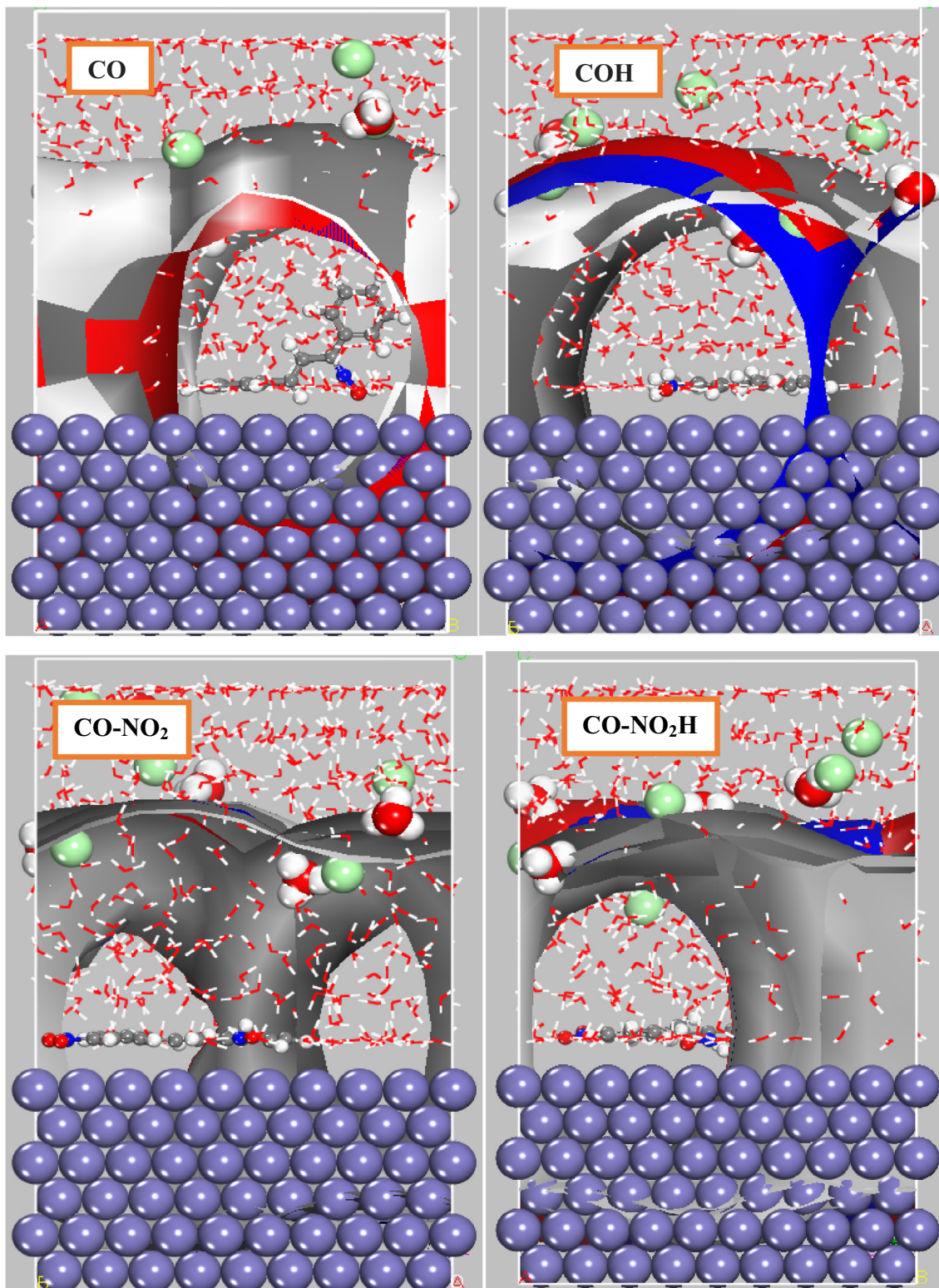


Fig.16. MD snapshots and density field distributions of the preferred adsorption configuration of the molecules studied in the neutral and protonated forms on the first well-ordered layer of iron.

$$E_{\text{interaction}} = E_{\text{total}} - (E_{\text{surface+solution}} + E_{\text{inhibitor}}) \quad (20)$$

Based on the simulation data to calculate the interaction energy ($E_{\text{interaction}}$), the values of this descriptor are collected in [Table 8](#). The negative value of $E_{\text{interaction}}$ confirms a large spontaneous adsorption of the selected molecules on the Fe (1 1 0) substrate

[79–82]. Thus, neutral and protonated inhibitors tend to adsorb in the acid solution thermodynamically on the Fe of the steel in question. The minimum value of COH shows that this molecule reacts strongly with the iron surface. This data validates the results obtained by the experiments.

Table 8E_{interaction} of systems inhibitors/Fe (1 1 0).

Systems (inhibitors/Fe(1 1 0))	E _{interaction} (kJ/mol)
CO/Fe(1 1 0)	-800.234
COH/Fe(1 1 0)	-889.390
CO-NO ₂ /Fe(1 1 0)	-811.653
CO-NO ₂ H/Fe(1 1 0)	-877.345

4. Conclusion

- Coupling between chemical and electrochemical techniques revealed that CO is a good corrosion inhibitor for carbon steel in 1 M HCl than CO-NO₂.
- PDP measurements indicated that the inhibitors act as a mixed type.
- The temperature effect and the activation parameters implied that CO and CO-NO₂ was chemisorbed onto the surface.
- The adsorption process occurred in compliance with Langmuir's adsorption isotherm model for the both inhibitors.
- SEM surface analysis exhibited a good coverage of CO and CO-NO₂ molecules on steel surface and evinced that these compounds prevent remarkably steel corrosion by the formation of a thin but very protective film.
- UV-vis studies confirmed the chemical interaction of the inhibitors with the carbon steel surface.
- The local reactivity and distribution of the electronic density of HOMO and LUMO show that the CO and CO-NO₂ contain highly reactive sites distributed throughout the molecular structure which are the cause of their inhibitory properties,
- Molecular dynamics simulations reveal the strong interaction between the CO and CO-NO₂ and the iron surface.

CRedit authorship contribution statement

A. Thoume: Data curation, Formal analysis, Investigation, Methodology, Writing - original draft. **D. Benmessaoud Left:** Conceptualization, Data curation, Formal analysis, Methodology, Writing - review & editing. **A. Elmakssoudi:** Conceptualization, Data curation, Formal analysis, Methodology, Writing - original draft. **F. Benhiba:** Software, Conceptualization, Data curation, Visualization, Writing - original draft. **A. Zarrouk:** Conceptualization, Formal analysis, Software, Supervision, Validation, Visualization, Writing - review & editing. **N. Benzbiria:** Conceptualization, Data curation, Formal analysis, Methodology. **I. Warad:** Conceptualization, Data curation, Visualization, Writing - original draft, Writing - review & editing. **M. Dakir:** Formal analysis, Investigation, Supervision, Writing - review & editing. **M. Azzi:** Investigation, Methodology, Project administration, Resources, Supervision, Validation, Visualization, Writing - original draft, Writing - review & editing. **M. Zertoubi:** Investigation, Methodology, Project administration, Resources, Supervision, Validation, Visualization, Writing - original draft, Writing - review & editing.

Declaration of Competing Interest

The authors declare that they have no known competing financial interests or personal relationships that could have appeared to influence the work reported in this paper.

References

- [1] Y. El Bakri, L. Guo, E.H. Anouar, E.M. Essassi, Electrochemical, DFT and MD simulation of newly synthesized triazolotriazine derivatives as corrosion inhibitors for carbon steel in 1M HCl, *J. Mol. Liq.* 274 (2019) 759–769.
- [2] J. Saranya, F. Benhiba, N. Anusuya, A. Ram Subbiah, S. Chitra Zarrouk, Experimental and computational approaches on the pyran derivatives for acid corrosion, *Colloids Surf., A* 603 (2020) 125231.
- [3] S. Rajendraprasad, S. Ali, B.M. Prasanna, Electrochemical Behavior of N1-(3-Methylphenyl)Piperidine-1,4-Dicarboxamide as a Corrosion Inhibitor for Soft-Cast Steel Carbon Steel in 1 M HCl, *J. Fail. Anal. and Preven* 20 (2020) 235–241.
- [4] H.B. Mahood, A.H. Sayer, A.H. Mekky, A.A. Khadom, Performance of Synthesized Acetone Based Inhibitor on Low Carbon Steel Corrosion in 1 M HCl Solution, *Chem. Afr.* 3 (2019) 263–276.
- [5] M.A. Bedair, A.S. Fouda, M.A. Ismail, A. Mostafa, Inhibitive effect of bithiophene carbonitrile derivatives on carbon steel corrosion in 1 M HCl solution: experimental and theoretical approaches, *Ionics* 25 (2019) 2913–2933.
- [6] S.M. Shaban, N-(3-(dimethyl benzyl ammonio) propyl) alkanamide chloride derivatives as corrosion inhibitors for mild steel in 1M HCl solution: experimental and theoretical investigation, *RSC Adv.* 6 (2016) 39784–39800.
- [7] A. Khadraoui, A. Khelifa, M. Hadjmeliiani, R. Mehdaou, K. Hachama, A. Tidu, Z. Azari, I.B. Obot, A. Zarrouk, Extraction, characterization and anti-corrosion activity of Mentha pulegium oil: Weight loss, electrochemical, thermodynamic and surface studies, *J. Mol. Liq.* 216 (2016) 724–731.
- [8] L. Afia, R. Salghi, E.H. Bazzi, A. Zarrouk, B. Hammouti, M. Bouri, H. Zarrouk, L. Bazzi, L. Bammou, Argan hulls extract: green inhibitor of mild steel corrosion in 1 M HCl solution, *Res. Chem. Intermed.* 38 (2012) 1707–1717.
- [9] S. Satpati, S. Kr, A. Saha, P. Suhasaria, D. Sukul Banerjee, Adsorption and anti-corrosion characteristics of vanillin Schiff bases on mild steel in 1 M HCl: experimental and theoretical study, *RSC Adv.* 10 (2020) 9258–9273.
- [10] A. Dutta, S. Kr, U. Saha, P. Adhikari, D. Sukul Banerjee, Effect of substitution on corrosion inhibition properties of 2-(substituted phenyl) benzimidazole derivatives on mild steel in 1 M HCl solution: a combined experimental and theoretical approach, *Corros. Sc.* 123 (2017) 256–266.
- [11] Q.H. Zhang, B.S. Hou, Y.Y. Li, G.Y. Zhu, H.F. Liu, G.A. Zhang, Two novel chitosan derivatives as high efficient eco-friendly inhibitors for the corrosion of mild steel in acidic solution, *Corros. Sc.* 164 (2019) 108346.
- [12] A. Thoume, A. Elmakssoudi, D. Benmessaoud Left, N. Benzbiria, F. Benhiba, M. Dakir, M. Zahouily, A. Zarrouk, M. Azzi, M. Zertoubi, Amino acid structure analog as a corrosion inhibitor of carbon steel in 0.5 M H₂SO₄: Electrochemical, synergistic effect and theoretical studies, *Chem. Data Collect.* 30 (2020) 100586.
- [13] A. Dehghani, A.H. Mostafatabar, G. Bahlakeh, B. Ramezanzadeh, M. Ramezanzadeh, Detailed-level computer modeling explorations complemented with comprehensive experimental studies of Quercetin as a highly effective inhibitor for acid-induced steel corrosion, *J. Mol. Liq.* 309 (2020) 113035.
- [14] K. Hu, J. Zhuang, J. Ding, Z. Ma, F. Wang, Xianguang Zeng, Influence of biomacromolecule DNA corrosion inhibitor on carbon steel, *Corros. Sc.* 125 (2017) 68–76.
- [15] E.A. Şahin, F. Tezcan, R. Solmaz, G. Kardeş, Inhibitive effect of 4-amino-N-benzylidenebenzamide Schiff base on mild steel corrosion in HCl solution, *J. Adhes. Sci. Technol.* 34 (2) (2020) 135–152.
- [16] H. Zhu, X. Chen, X. Li, J. Wang, Z. Hu, X. Ma, 2-aminobenzimidazole derivative with surface activity as corrosion inhibitor of carbon steel in HCl: Experimental and theoretical study, *J. Mol. Liq.* 297 (2020) 111720.
- [17] I. Benmahammed, T. Douadi, S. Issaadi, M. Al-Noaimi, S. Chafaa, Heterocyclic Schiff bases as corrosion inhibitors for carbon steel in 1 M HCl solution: hydrodynamic and synergetic effect, *J. Dispersion Sci. Technol.* 41 (7) (2020) 1002–1021.
- [18] A. Zarrouk, B. Hammouti, H. Zarrok, R. Salghi, A. Dafali, Lh. Bazzi, L. Bammou, S. S. Al-Deyab, Electrochemical impedance spectroscopy and weight loss study for new pyridazine derivative as inhibitor for copper in nitric acid, *Der Pharma Chem.* 4 (1) (2012) 337–346.
- [19] B. Hammouti, A. Zarrouk, S.S. Al-Deyab, I. Warad, Temperature Effect, Activation Energies and Thermodynamics of Adsorption of ethyl 2-(4-(2-ethoxy-2-oxoethyl)-2-pTolylquinoxalin-1(4H)-yl)Acetate on Cu in HNO₃, *Orient. J. Chem.* 27 (1) (2011) 23–31.
- [20] Y. Qiang, S. Zhang, L. Wang, Understanding the adsorption and anticorrosive mechanism of DNA inhibitor for copper in sulfuric acid, *Appl. Surf. Sci.* 492 (2019) 228–238.
- [21] H. Zarrok, A. Zarrouk, R. Salghi, H. Oudda, B. Hammouti, M. Assouag, M. Taleb, M. Ebn Touhami, M. Bouachrine, S. Boukhris, Gravimetric and quantum chemical studies of 1-[4-acetyl-2-(4-chlorophenyl)quinoxalin-1(4H)-yl] acetone as corrosion inhibitor for carbon steel in hydrochloric acid solution, *J. Chem. Pharm. Res.* 4 (12) (2012) 5056–5066.
- [22] N. Kovacevic, A. Kokalj, Chemistry of the interaction between azole type corrosion inhibitor molecules and metal surfaces, *Mater. Chem. Phys.* 137 (2012) 331–339.
- [23] A. Salhi, S. Tighadouini, M. El-Massaoudi, M. Elbelghiti, A. Bouyanzer, S. Radi, S. El Barkany, F. Bentiss, A. Zarrouk, Keto-enol heterocycles as new compounds of corrosion inhibitors for carbon steel in 1 M HCl: Weight loss, electrochemical and quantum chemical investigation, *J. Mol. Liq.* 248 (2017) 340–349.
- [24] Y. Luo, R. Song, Y. Li, S. Zhang, Z.-Jun Liu, J. Fu, H.-Liang Zhu, Design, synthesis, and biological evaluation of chalcone oxime derivatives as potential immunosuppressive agents, *Bioorg. Med. Chem. Lett.* 22 (2012) 3039–3043.
- [25] S. Fandakli, İ.S. Doğan, H.E. Sellitepe, A. Yaşar, N. Yaylı, Synthesis, theoretical calculation and α-glucosidase inhibition of new chalcone oximes, *Org. Commun.* 11 (1) (2018) 23–34.
- [26] D.S. Bolotin, N.A. Bokach, M.Y. Demakova, V.Y. Kukushkin, Metal-Involving Synthesis and Reactions of Oximes, *Chem. Rev.* 117 (2017) 13039–13122.

- [27] S.K. Radhakrishnan, R.G. Shimmom, C. Conn, A.T. Baker, Evaluation of Novel Chalcone Oximes as Inhibitors of Tyrosinase and Melanin Formation in B16 Cells, *Arch. Pharm. Chem. Life Sci.* 349 (2016) 20–29.
- [28] A.K. Surowiak, S. Lochynski, D.J. Strub, Unsubstituted Oximes as Potential Therapeutic Agents, *Symmetry* 12 (2020) 575.
- [29] X. Xu, J. Li, C. Du, Y. Song, Improved Synthesis of 1,3-Diaryl-2-propen-1-one Oxime in the Presence of Anhydrous Sodium Sulfate, *Chin. J. Chem.* 29 (12) (2011) 2781–2784.
- [30] M. Mobin, M. Rizvi, Polysaccharide from *Plantago* as a Green Corrosion Inhibitor for Carbon Steel in 1 M HCl Solution, *Carbohydr. Polym.* 160 (2017) 172–183.
- [31] H. Ouici, M. Tourabi, O. Benali, C. Selles, C. Jama, A. Zarrouk, F. Bentiss, Adsorption and corrosion inhibition properties of 5-amino 1,3,4-thiadiazole-2-thiol on the mild steel in hydrochloric acid medium: Thermodynamic, surface and electrochemical studies, *J. Electroanal. Chem.* 803 (2017) 125–134.
- [32] Y. Kharbach, F.Z. Qachchachi, A. Haoudi, M. Tourabi, A. Zarrouk, C. Jama, L.O. Olasunkanmi, E.E. Ebenso, F. Bentiss, Anticorrosion performance of three newly synthesized isatin derivatives on carbon steel in hydrochloric acid pickling environment: Electrochemical, surface and theoretical studies, *J. Mol. Liq.* 246 (2017) 302–316.
- [33] F. Benhiba, Y. ELaoufir, M. Belayachi, H. Zarrok, A. El Assry, A. Zarrouk, B. Hammouti, E.E. Ebenso, A. Guenbour, S.S. Al Deyab, H. Oudda, Theoretical and experimental studies on the inhibition of 1,1'-(2-phenylquinoxaline 1,4-diyl) diethanone for the corrosion of carbon steel in 1.0 M HCl, *Der Pharm. Lett.* 6 (4) (2014) 306–318.
- [34] E. Alibakhshi, M. Ramezanzadeh, G. Bahlakeh, B. Ramezanzadeh, M. Mahdavian, M. Motamedi, *Glycyrrhiza glabra* leaves extract as a green corrosion inhibitor for mild steel in 1 M hydrochloric acid solution: Experimental, molecular dynamics, Monte Carlo and quantum mechanics study, *J. Mol. Liq.* 255 (2018) 185–198.
- [35] L.O. Olasunkanmi, B.P. Moloto, I.B. Obot, E.E. Ebenso, Anticorrosion studies of some hydantoin derivatives for mild steel in 0.5 M HCl solution: Experimental, quantum chemical, Monte Carlo simulations and QSAR studies, *J. Mol. Liq.* 252 (2018) 62–74.
- [36] A. Saady, F. El-Hajjaji, M. Taleb, K. Ismaili Alaoui, A. El Biache, A. Mahfoud, G. Alhouari, B. Hammouti, D.S. Chauhan, M.A. Quraishi, Experimental and theoretical tools for corrosion inhibition study of mild steel in aqueous hydrochloric acid solution by new Indanones derivatives, *Mater. Discovery* 12 (2018) 30–42.
- [37] M. Rbaa, F. Benhiba, M. Galai, Ashraf S. Abousalem, M. Ouakki, B. Chin-Hung Lai, C. Lakhri, I. Jama, M. Warad, A. Zarrouk EbnTouhami, Synthesis and characterization of novel Cu (II) and Zn (II) complexes of 5-[[2-(2-hydroxyethyl) sulfanyl] methyl]-8-hydroxyquinoline as effective acid corrosion inhibitor by Experimental and Computational testings, *Chem. Phys. Lett.* 754 (2020) 137771.
- [38] *Materials Studio, Revision 8.0, Accelrys Inc., San Diego, USA* (2016).
- [39] H.C. Andersen, Molecular dynamics simulations at constant pressure and/or temperature, *J. Chem. Phys.* 72 (1980) 2384–2393.
- [40] B. El-Dien, M. El-Gendya, S.T. Atwaa, A.A. Ahmed, A.Y. El-Etre, Synthesis and Characterization of Carbon Steel Corrosion Inhibitors Based on 4,5,6,7-tetrahydrobenzo[b]thiophene Scaffold, *Prot. Met. Phys. Chem. Surf.* 55 (2019) 179–186.
- [41] R. Yıldız, Adsorption and inhibition effect of 2,4-diamino-6-hydroxypyrimidine for mild steel corrosion in HCl medium: experimental and theoretical investigation, *Ionics* 25 (2019) 859–870.
- [42] Y. El Ouadi, F. Abriqach, A. Bouyanzer, R. Touzani, O. Riant, B. ElMahi, A. El Assry, S. Radi, A. Zarrouk, B. Hammouti, Corrosion inhibition of mild steel by new N-heterocyclic compound in 1 M HCl: Experimental and computational study, *Der Pharma Chem.* 7 (8) (2015) 265–275.
- [43] Y.E. Louadi, F. Abriqach, A. Bouyanzer, R. Touzani, A. El Assry, A. Zarrouk, B. Hammouti, Theoretical and Experimental Studies on the Corrosion Inhibition Potentials of Two Tetrakis Pyrazole Derivatives for Mild Steel in 1.0 M HCl, *Port. Electrochim. Acta* 35 (3) (2017) 159–178.
- [44] H. Derfouf, Y. Harek, L. Larabi, W. Jeffrey, B.M. Ladan, Corrosion inhibition activity of carbon steel in 1.0 M hydrochloric acid medium using *Hammada scoparia* extract: gravimetric and electrochemical study, *J. Adhes. Sci. Technol.* 33 (8) (2019) 808–833.
- [45] C. Verma, L.O. Olasunkanmi, I.B. Obot, E.E. Ebenso, M.A. Quraishi, 2, 4-diamino-5-(phenylthio)-5H-chromeno [2, 3-b] pyridine-3-carbonitriles as green and effective corrosion inhibitors: gravimetric, electrochemical, surface morphology and theoretical studies, *RSC Adv.* 6 (2016) 53933–53948.
- [46] J. Radilla, G.E. Negron-Silva, M. Palomar-Pardave, M. Romero-Romo, M. Galvan, DFT study of the adsorption of the corrosion inhibitor 2-mercaptopimidazole onto Fe (100) surface, *Electrochim. Acta* 112 (2013) 577–586.
- [47] N. Anusuya, J. Saranya, P. Sounthari, A. Zarrouk, S. Chitra, Corrosion inhibition and adsorption behaviour of some bis-pyrimidine derivatives on mild steel in acidic medium, *J. Mol. Liq.* 225 (2017) 406–417.
- [48] A. Boutouil, M.R. Laamari, I. Elazhary, L. Bahsis, H. Anane, S.-E. Stiriba, Towards a deeper understanding of the inhibition mechanism of a new 1,2,3-triazole derivative for mild steel corrosion in the hydrochloric acid solution using coupled experimental and theoretical methods, *Mater. Chem. Phys.* 241 (2019) 122420.
- [49] M. El Hezzat, M. Assouag, H. Zarrok, Z. Benzekri, A. El Assry, S. Boukhris, A. Souizi, M. Galai, R. Touri, M. Ebn Touhami, H. Oudda, A. Zarrouk, Correlated DFT and electrochemical study on inhibition behavior of ethyl 6-amino-5-cyano-2-methyl-4-(p-tolyl)-4H-pyran-3-carboxylate for the corrosion of mild steel in HCl, *Der Pharma Chem.* 7 (10) (2015) 77–88.
- [50] M. Khattabi, F. Benhiba, S. Tabti, A. Djedouani, A. El Assry, R. Touzani, I. Warad, H. Oudda, A. Zarrouk, Performance and computational studies of two soluble pyran derivatives as corrosion inhibitors for mild steel in HCl, *J. Mol. Struct.* 1196 (2019) 231–244.
- [51] A. Popova, E. Sokolova, S. Raicheva, M. Christov, AC and DC study of the temperature effect on mild steel corrosion in acid media in the presence of benzimidazole derivatives, *Corros. Sci.* 45 (2003) 33–58.
- [52] M. Rbaa, F. Benhiba, I.B. Obot, H. Oudda, I. Warad, B. Lakhri, A. Zarrouk, Two new 8-hydroxyquinoline derivatives as an efficient corrosion inhibitors for mild steel in hydrochloric acid: Synthesis, electrochemical, surface morphological, UV-visible and theoretical studies, *J. Mol. Liq.* 276 (2019) 120–133.
- [53] M.A. Deyab, R. Ouarsal, M. Lachkar, B. El Bali, R. Essehli, Phosphites compound: Novel corrosion inhibitor for radioactive waste container (carbon steel) in simulated Callovo-Oxfordian (COx) groundwater, *J. Mol. Liq.* 219 (2016) 994–999.
- [54] I. Hamdani, E. El Ouariachi, O. Mokhtari, A. Salhi, N. Chahboun, B. ElMahi, A. Bouyanzer, A. Zarrouk, B. Hammouti, J. Costa, Chemical constituents and corrosion inhibition of mild steel by the essential oil of *Thymus algeriensis* in 1.0 M hydrochloric acid solution, *Der Pharma Chem.* 7 (8) (2015) 252–264.
- [55] A. Tazouti, M. Galai, R. Touri, M. Ebn Touhami, A. Zarrouk, Y. Ramli, M. Saraçoğlu, S. Kaya, F. Kandemirli, C. Kaya, Experimental and theoretical studies for mild steel corrosion inhibition in 1.0 M HCl by three new quinoxaline derivatives, *J. Mol. Liq.* 221 (2016) 815–832.
- [56] H. Zarrok, A. Zarrouk, R. Salghi, H. Oudda, B. Hammouti, M. Ebn, M. Bouachrine Touhami, S. Boukhris, A Combined Experimental and Theoretical Study on the Corrosion Inhibition and Adsorption Behaviour of Quinoxaline Derivative During Carbon Steel Corrosion in Hydrochloric Acid, *Port. Electrochim. Acta* 30 (6) (2012) 405–417.
- [57] A. Keleşoğlu, R. Yıldız, İ. Dehri, 1-(2-Hydroxyethyl)-2-imidazolidinone as corrosion inhibitor of mild steel in 0.5 M HCl solution: thermodynamic, electrochemical and theoretical studies, *J. Adhes. Sci. Technol.* 33 (18) (2019) 2010–2030.
- [58] Z. Hu, Y. Meng, X. Ma, H. Zhu, J. Li, C. Li, D. Cao, Experimental and theoretical studies of benzothiazole derivatives as corrosion inhibitors for carbon steel in 1 M HCl, *Corros. Sci.* 112 (2016) 563–575.
- [59] S. Hu, A. Guo, Y. Geng, X. Jia, S. Sun, J. Zhang, Synergistic effect of 2-oleyl-1-oleylamidoethyl imidazole ammonium methylsulfate and halide ions on the inhibition of mild steel in HCl, *Mater. Chem. Phys.* 134 (2012) 54–60.
- [60] M. El Faydy, M. Galai, M. Ebn Touhami, I.B. Obot, B. Lakhri, A. Zarrouk, Anticorrosion potential of some 5-amino-8-hydroxyquinolines derivatives on carbon steel in hydrochloric acid solution: Gravimetric, electrochemical, surface morphological, UV-visible, DFT and Monte Carlo simulations, *J. Mol. Liq.* 248 (2017) 1014–1027.
- [61] M. Rbaa, M. Ouakki, M. Galai, A. Berisha, B. Lakhri, C. Jama, I. Warad, A. Zarrouk, Simple preparation and characterization of novel 8-Hydroxyquinoline derivatives as effective acid corrosion inhibitor for mild steel: Experimental and theoretical studies, *Colloids Surf., A* 602 (2020) 125094.
- [62] D.K. Yadav, M.A. Quraishi, Application of Some Condensed Uracils as Corrosion Inhibitors for Mild Steel: Gravimetric, Electrochemical, Surface Morphological, UV-Visible, and Theoretical Investigations, *Ind. Eng. Chem. Res.* 51 (46) (2012) 14966–14979.
- [63] *MarvinSketch Software, Version: 18.22, ChemAxon Ltd., 2018.*
- [64] L. Saqalli, M. Galai, F. Benhiba, N. Gharda, N. Habbadi, R. Ghailane, M. Ebn Touhami, Y. Peres-luchese, A. Souizi, R. Touri, Experimental and theoretical studies of Alizarin as corrosion inhibitor for mild steel in 1.0 M HCl solution, *J. Mater. Environ. Sci.* 8 (7) (2017) 2455–2467.
- [65] B. Tan, S. Zhang, H. Liu, Y. Qiang, W. Li, L. Guo, S. Chen, Insights into the inhibition mechanism of three 5-phenyltetrazole derivatives for copper corrosion in sulfuric acid medium via experimental and DFT methods, *J. Taiwan Inst. Chem. Eng.* 102 (2019) 424–437.
- [66] A. El yaktini, A. Lachiri, M. El Faydy, F. Benhiba, H. Zarrok, M. El Azzouzi, M. Zertoubi, M. Azzi, B. Lakhri, A. Zarrouk, Inhibitor effect of new azomethine derivative containing an 8-hydroxyquinoline moiety on corrosion behavior of mild carbon steel in acidic media, *Int. J. Corros. Scale Inhib.* 7 (4) (2017) 609–632.
- [67] R. Hissou, F. Benhiba, M. Khudhair, M. Berradi, A. Mahsoun, H. Oudda, A. El Harfi, I.B. Obot, A. Zarrouk, Investigation and comparative study of the quantum molecular descriptors derived from the theoretical modeling and Monte Carlo simulation of two new macromolecular polyepoxide architectures TGEEBA and HGEMDA, *J. King Saud Univ. Sci.* 667–676 (2020).
- [68] F.E. Awe, S.O. Idris, M. Abdulwahab, E.E. Oguzie, Theoretical and experimental inhibitive properties of mild steel in HCl by ethanolic extract of *Boscia senegalensis*, *Cogent Chem.* 1 (2015) 1112676.
- [69] T. Laabaissi, F. Benhiba, Z. Rouifi, M. Missiou, K. Ourrak, H. Oudda, Y. Ramli, I. Warad, M. Allali, A. Zarrouk, New quinoxaline derivative as a green corrosion inhibitor for mild steel in mild acidic medium: Electrochemical and theoretical studies, *Int. J. Corros. Scale Inhib.* 8 (2) (2019) 241–256.
- [70] O. Fergachi, F. Benhiba, M. Rbaa, R. Touri, M. Ouakki, M. Galai, B. Lakhri, H. Oudda, M. Ebn Touhami, Experimental and Theoretical Study of Corrosion Inhibition of Mild Steel in 1.0 M HCl Medium by 2-(4-(chloro phenyl)-1H-benzimidazol)-1-yl)phenyl)methanone), *Mater. Res.* 21 (6) (2018) e20171038.
- [71] F. Benhiba, Z. Benzekri, A. Guenbour, M. Tabyaoui, A. Bellaouchou, S. Boukhris, H. Oudda, I. Warad, A. Zarrouk, Combined electronic/atomic level

- computational, surface (SEM/EDS), chemical and electrochemical studies of the mild steel surface by quinoxalines derivatives anti-corrosion properties in 1 mol. L-1 HCl solution, *Chin. J. Chem. Eng.* 28 (5) (2020) 1436–1458.
- [72] A. Kokalj, Is the analysis of molecular electronic structure of corrosion inhibitors sufficient to predict the trend of their inhibition performance, *Electrochim. Acta* 56 (2010) 745–755.
- [73] N. Kovačević, A. Kokalj, Analysis of molecular electronic structure of imidazole-and benzimidazole-based inhibitors: a simple recipe for qualitative estimation of chemical hardness, *Corros. Sci.* 53 (2011) 909–921.
- [74] A. El yaktini, A. Lachiri, M. El Faydy, F. Benhiba, H. Zarrok, M. El Azzouzi, M. Zertoubi, M. Azzi, B. Lakhri, A. Zarrouk, Practical and Theoretical Study on the Inhibitory Influences of New Azomethine Derivatives Containing 8-hydroxyquinoline Moiety for the Corrosion of Carbon Steel in 1 M HCl, *Orient. J. Chem.* 34 (6) (2018) 3016–3029.
- [75] K. Cherrak, F. Benhiba, N.K. Sebbar, E.M. Essassi, M. Taleb, A. Zarrouk, A. Dafali, Corrosion inhibition of mild steel by new Benzothiazine derivative in a hydrochloric acid solution: Experimental evaluation and theoretical calculations, *Chem. Data Collect.* 22 (2019) 100252.
- [76] M. Rbaa, F. Benhiba, R. Hssisou, Y. Lakhri, B. Lakhri, M. Ebn Touhami, I. Warad, A. Zarrouk, Green synthesis of novel carbohydrate polymer chitosan oligosaccharide grafted on D-glucose derivative as bio-based corrosion inhibitor, *J. Mol. Liq.* 322 (2021) 114549.
- [77] A. Berrissoul, A. Ouahach, F. Benhiba, A. Romane, A. Zarrouk, A. Guenbour, B. Dikici, A. Dafali, Evaluation of *Lavandula mairei* extract as green inhibitor for mild steel corrosion in 1 M HCl solution. Experimental and theoretical approach, *J. Mol. Liq.* 313 (2020) 113493.
- [78] S.K. Saha, P. Ghosh, A. Hens, N.C. Murmu, P. Banerjee, Density functional theory and molecular dynamics simulation study on corrosion inhibition performance of mild steel by mercapto-quinoline Schiff base corrosion inhibitor, *Phys. E Low-Dimens. Syst. Nanostructures.* 66 (2015) 332–341.
- [79] M. Rbaa, F. Benhiba, P. Dohare, L. Lakhri, R. Tourir, B. Lakhri, A. Zarrouk, Y. Lakhri, Synthesis of new epoxy glucose derivatives as a non-toxic corrosion inhibitors for carbon steel in molar HCl: Experimental, DFT and MD simulation, *Chem. Data Collect.* 27 (2020) 100394.
- [80] H. Rahmani, K.I. Alaoui, M. EL Azzouzi, F. Benhiba, A. El Hallaoui, Z. Rais, M. Taleb, A. Saady, B. Labriti, A. Aouniti, A. Zarrouk, Corrosion assessment of mild steel in acid environment using novel triazole derivative as a anti-corrosion agent: A combined experimental and quantum chemical study, *Chem. Data Collect.* 24 (2019) 100302.
- [81] L.O. Olasunkanmi, I.B. Obot, E.E. Ebenso, Adsorption and corrosion inhibition properties of N-{n-[1-R-5-(quinoxalin-6-yl)-4, 5-dihydropyrazol-3-yl] phenyl} methanesulfonamides on mild steel in 1 M HCl: experimental and theoretical studies, *RSC Adv.* 6 (2016) 86782–86797.
- [82] F. Benhiba, R. Hsissou, Z. Benzekri, M.E. Belghiti, A. Lamhamdi, A. Bellaouchou, A. Guenbour, S. Boukhris, H. Oudda, I. Warad, A. Zarrouk, Nitro substituent effect on the electronic behavior and inhibitory performance of two quinoxaline derivatives in relation to the corrosion of mild steel in 1 M HCl, *J. Mol. Liq.* 312 (2020) 113367.